Summer 8-1-2023

# Projecting Vegetation Condition and Fire Risk in Southern California

Westin K. Guthrie
*University of New Mexico*

Westin Guthrie

*Candidate*

Geography

*Department*

This thesis is approved, and it is acceptable in quality and form for publication:

*Approved by the Thesis Committee:*

Chris Lippitt , Chairperson

Daniel Krofcheck

Chris Duvall

Zachary Robbins

# PROJECTING VEGETATION CONDITION AND FIRE RISK IN SOUTHERN CALIFORNIA

**by**

**WESTIN GUTHRIE**

**BACHELORS OF SCIENCE, GEOGRAPHY, UNM, 2019**

THESIS

Submitted in Partial Fulfillment of the
Requirements for the Degree of

**Masters of Science**

**Geography**

The University of New Mexico
Albuquerque, New Mexico

**August, 2023**

**PROJECTING VEGETATION CONDITION AND FIRE RISK IN SOUTHERN CALIFORNIA**

**By**

**Westin Guthrie**

**B.S., Geography, The University of New Mexico, 2019**
**M.S., Geography, The University of New Mexico, 2023**

## ABSTRACT

In the western US, relationships between fire, vegetation, climate, and urban areas are dynamic and evolving. This work used a forest landscape model, LANDIS-II, informed by future climate scenarios and projections of urban expansion to understand wildfire interactions within projected Wildland Urban Interface (WUI) areas. This simulation showed that in both 2050 and 2100 +93% of the WUI in southern California experienced fire. Future work needs to be done in parametrizing forest biomass to ensure the validity of projections. Additionally, increasing each climate scenario model's replicates will create more accurate projections.

## TABLE OF CONTENTS

# LIST OF FIGURES

# LIST OF TABLES

## LIST OF EQUATIONS

$$biomass = \text{'}CARBON\_AG\text{'}/.5 * \text{'}TPA\_UNADJ\text{'}$$ eq. 1 –

Where biomass is in lbs/acre, 'CARBON_AG' is above ground carbon measured in pounds and 'TPA_UNADJ' is a value that must be multiplied to understand per acre information with both variables from the Forest Inventory and Analysis program.

$$biomass\ g/m2 = biomass\ lbs/acre * .112085$$ eq. 2 -

Converting biomass generated by eq. 1 to g/m$^2$.

$$OLS = \text{'}AGEDIA \sim DIA * HT\text{'}$$ eq. 3–

OLS equation used to obtain coefficients used to inform age (eq. 4).

$$ages = OLS\_coefficient.DIA * diameters + OLS\_coefficient.HT * heights + OLS\_coefficient.DIA{:}HT * diameters * heights + OLS\_coefficient.intercept$$ eq. 4 –

Model type *a* ages equation used to determine species age informed by variables acquired from eq. 3.

$$age = (6.69 * x) + 18.5\ (Gascho\ Landis\ and\ Bailey\ 2006)$$ eq. 5 –

Age equation for pinyon species where *x* is diameter in centimeters.

$$age = 1.5519(x) - 29.819\ (Barry\ 2014)$$ eq. 6 –

Model type *e* age equation for California Laurel where x is diameter in centimeters.

$$age = (0.4667 * x) + 31.0326\ (Brotherson, Davis, and\ Greenwood\ 1980)$$ eq. 7 –

Model type *f* age equation for curlleaf mountain-mahogany where x is diameter in millimeters.

$$Bark\ Thickness\ =\ Vsp(D)$$ eq. 8 –

Where Vsp is the species multiplier provided by FEE-FVS and D is species diameter in inches provided from FIA data.

$$Bark\ Thickness\ =\ D/2\ (1-k)$$ (Kozak and Yang 1981) eq. 9 –

Where *d* is diameter at breast height outside bark (DHOB), and *k* the regression coefficient for the relationship of diameter inside bark (DIB, d) to DOB.

$$\sqrt{BarkThickness} = a * \sqrt{DBH}$$ (Zeibig-Kichas et al. 2016) eq. 10 –

Where *a* and b are a species related coefficient and DBH is diameter at breast height.

$$Bark\ Thickness = -1.693 + 0.0219x + 1.2813x^{-1}$$ (McDonald 1983) eq. 11 –

Where Vsp is the species multiplier provided by FEE-FVS and D is species diameter in inches provided from FIA data.

$$Bark\ Thickness\ (mm) =\ 0.835 * x^{0.797}$$ (Schafer et al. 2015) eq. 12 –

Where x is DIA in centimeters.

## 1.0 Introduction

In the western United States, there has been a notable increase in stand-replacing fires as the mean and the maximum fire size and annually burned area have dramatically increased since the 1980s (Miller et al. 2009). During 1972 – 2018, California, U.S. experienced a fivefold increase in annual burned area, this increase was primarily supported from an eightfold increase in summer forest-fire extent (Williams et al. 2019). Starting in the early 20$^{th}$ century fire suppression has created altered fire regimes and has affected forest health in California (Nigro and Molinari 2019). Trends of rising regional temperature (Miller et al. 2009) and an autumn precipitation reduction of ~30% over the last four decades, aggregate fire weather indices have increased by +20% (Goss et al. 2020) indicating a higher fire risk in California. Recent estimates suggest that more than 100 million trees have died in California since 2010, primarily in the southern and central Sierra Nevada areas (Stephens et al. 2018). The magnitude of this level of mortality in the region presents such a large and greater potential for “mass fire” to exist in the coming decades, driven by the dry, combustible, large woody material that produces severe fires (Stephens et al. 2018). As an increasing vapor pressure deficit becomes more prominent in southern California, fine fuels and small wood debris will experience even lower moisture content, boosting the ability of fire spread (Balch et al. 2022). Kramer et al. 2018 found that over three decades the WUI contained 50% of buildings destroyed by wildfire. It is vital to understand fire in California and how that

relationship interacts with vegetation and climate to accurately project possible future fire risks for southern California wildland-urban interface.

The question this work sought to answer is:

*How will contemporary and future climate scenarios impact the frequency and severity of fire intersecting with an expanding wildland-urban interface (WUI) in southern California?*

Sub-question:

*How do different climate models impact WUI fire severity and frequency?*

This research examined how vegetation and fire interact within southern California through contemporary climate scenarios and possible futures modeled in the Multivariate Adaptive Constructed Analogs (MACA) CMIP5 Statistically Downscaled Climate Projections of three global climate models using the future Representative Concentration Pathway (RCP 8.5) scenario for 2019-2100. This is a large landscape (4,816,319 ha) where fire has the potential to impact millions of people. A better understanding of the interactions of climate and fire can influence development decisions and has the power to alter fire management regimes through the knowledge of where and what treatments are effective.

To understand these complex relationships between fire, climate, and vegetation a forest landscape model, LANDIS-II, was applied to the area of interest. LANDIS-II is capable of simulating forest growth, succession, and natural or human disturbances (Krofcheck et al. 2017, Liang et al. 2017, Syphard et al. 2011). The

LANDIS-II forests succession extension Net Ecosystem Carbon and Nitrogen (NECN), which was designed to provide total ecosystem accounting of carbon and nitrogen, allows species to respond dynamically to a changing climate through establishment and growth (Scheller et al. 2011). Social-Climate Related Pyrogenic Processes and their Landscape Effects (SCRPPLE), is used to simulate fire regime change due to climatic and social factors. Climate is represented through a Fire Weather Index and social processes are represented through suppression, accidental ignitions, and prescribed fire (Scheller et al. 2019). LANDIS-II allows us to create vegetation succession projections and project fire under different management regimes through manipulation of thinning and prescribed burn practices to understand how fire will interact with projected urban growth to the year 2100.

## 2.0 Background

The following sections will cover the foundational knowledge needed to understand fire through relationships among history, climate, current regimes, and vegetation within southern California and most importantly understand the feedbacks within the context of the region when modeling forest succession and disturbances with LANDIS-II.

## 2.1 Fire History in Southern California Ecosystems

Ecosystems in southern California have evolved to coexist with fire to maintain species composition (Syphard et al. 2007). However, anthropogenic intervention from climate change, fire exclusion, and increased human ignitions in

wildland-urban interface zones have resulted in natural ecosystem relationships with fire being disturbed, thus creating a mix of more frequent and less frequent fires relative to historical regimes (Safford and Stevens 2017). In these fire-adapted ecosystems, the changes in fire behavior are altering the ecosystems themselves (Syphard et al. 2007, Jacobsen et al. 2004, Van de Water and Safford 2011), resulting in a complex interdependency between fire behavior, ecosystem function, and anthropogenic activities.

### 2.1.1 Historic Fire Return Interval and Severity

The historic fire return interval in southern California ecosystems has been the subject of debate. Previous works held that pre-settlement fires in California chaparral environments were small and low intensity (Bonnicksen 1981, Minnich 1983, 1995) suggesting that lightning-ignited fires only burned small patches of 100-1000 hectares which would produce a mosaic of fuels to act as a fire spread barrier when a patch was burned. This is not likely the case as chaparral shrub landscapes in southern California have fuel characteristics that are conducive to high-severity fires that commonly reach 10,000 hectares or more (Keeley et al. 1999). These large, and historically infrequent high-intensity fires have existed in the area (Keeley and Zedler 2009). However, California's growth in population has also been accompanied by greater fire frequency within chaparral shrublands of southern California (Lippitt et al. 2012).

An increase in chaparral density, human population growth, and urban expansion has led to an increase in fire frequency beyond historical levels in some

areas (Syphard et al. 2007). A growing frequency of large high-intensity fires within forest ecosystems in California (Westerling et al. 2006) has been, in part, attributed to fire suppression and fire exclusion policies in western U.S. forests (Syphard et al. 2007, Vankat and Major 1978) and a rising in extreme fire weather days (Gross et al. 2020). Fire suppression and exclusion have resulted in fuel build-ups believed to be historically large and ahistoric tree densities (Safford and Stevens 2017, Gray et al. 2005) within mixed conifer forests leading to a greater likelihood of high-intensity crown fires (Gray et al. 2005). Within California shrubland ecosystems, large high-intensity crown fires are a natural feature aided by drought conditions and strong, dry, Santa Ana winds affecting coastal southern California (Keeley and Zedler 2009). The landscape in southern California has historically been subjected to high-intensity fires (Keeley and Zedler 2009), but the frequency has increased aided by increased drought and low humidity conditions due to climatic change in chaparral (Syphard et al. 2018).

Historic fire return intervals vary within California depending on the system. California shrublands have a natural fire-return interval of 30-150 years, in S. California it is generally closer to 30 years (Halsey and Keeley 2016). Many species within this community are pyroendemic, plants whose seedling germination and successful seedling recruitment are constrained to postfire environments (Keeley and Pausas 2018). Other species trigger germination by smoke (eg, *Emmenanthe penduliflora and Phacelia brachyloba*) creating a unique, endemic, biodiverse landscape. Chaparral species within their natural fire return have adapted to become resilient to fires, but increased fire frequency due to human-caused ignitions and

anthropogenic climate change can lead to the vigor and regeneration of these fire-adapted species being impacted. A return to a historic fire interval could allow species biodiversity to remain rich through seedbank deposits replenishing awaiting fire and smoke germination queues and allow keystone non-resprouting shrubs and resprouting-dominated chaparral stands to thrive after fire (Halsey and Keeley 2016).

While chaparral has been characterized by natural high-intensity crown fires with intervals of 30-150 years, pre-settlement California conifer forests in the Sierra Nevada's had regimes that yielded low-moderate severity fires which were frequent with occasional crown fires in mature trees Historical returns in mixed conifer systems were characterized by returns of 0 to 35 years with a heterogeneous pine-dominated makeup and a lower tree density than their modern counterparts these forests experienced more frequent fire invigorating understory fire-stimulated shrub species (Safford and Stevens 2017).

### 2.1.2 Modern Fire Regimes

Southern California has experienced a steady loss of shrub cover. Shrub loss has been aided by increased population density in southern California resulting in increased fire frequency and nitrogen deposition rates from atmospheric pollution (Talluto and Suding 2008) contributing to the loss of coastal shrubs and chaparral (CH). One study found that since 1953 woody cover experienced declines with a mean loss of 22.5% cover over 311 plots and 28% were fully type converted (Syphard et al. 2019). This deadly combination of both fire frequency and nitrogen

depositions rates creates an opportunity for non-native herbaceous colonizers, particularly annual grasses. Increased fire frequency does not allow resilient native, postfire endemic, species' soil-seed banks time to recharge with at least 15 or more years being suggested (Syphard et al. 2019) to gather enough seed numbers for recovery. A fire return of even 6 years can affect chaparral environments that recruit from seed banks where frequent fires contributed to a loss of 86.8% in non-sprouting species in one study (Jacobsen et al. 2004).

Mixed conifer systems were not characterized by high severity and intensity fires, unlike chaparral. Fire return intervals of 11 – 16 years of low-moderate severity (Safford and Stevens 2017) were common lowering fuels build-up and limiting forest density and thus intensity. Conifer systems have been impacted by fire exclusion policies which have lengthened fire return intervals to 35 to 200 years (Safford and Stevens 2017) with many southern California mixed conifer forests experiencing an average return of 77.8 years (Nigro and Molinari 2019). This average return, aided by a combination of climate change and fire management policies, has led to half of southern California mixed conifer forests not experiencing fire in the last 109 years (Nigro and Molinari 2019) creating conditions for increased fire severity. Increased severity fires in mixed conifer forests have made them vulnerable to stand replacement due to large patch mortality via the reduction of regeneration from seed dispersal, due to distance from seed source (Nigro and Molinari 2019). These forests are adapted to low and moderate-intensity fires. As the severity of fires increases, type conversion of forest to chaparral, hardwood forest, or grassland can

occur if areas are reburned before conifer species can reestablish (Steel et al. 2018, Lauvaux et al. 2016, Paudel et al. 2022).

Differences in fire intensity and frequency matter between chaparral and mixed conifer systems. Chaparral fires are high-intensity crown fires, and a high return interval leads to type conversion for those species. An increased fire frequency from a historic return of at least 30 years or more (Van de Water and Safford 2011) has been linked to type conversion in chaparral and shrubland communities (Lippitt et al. 2012). In mixed conifer forests, both frequency and intensity are drivers of dominant species type conversion. Climate change and fire exclusion strategies have led to forests developing hazardous fuel loads which help create high-intensity crown fires (Syphard et al. 2007) that lead to stand replacement (Miller et al. 2009). In many yellow pine-mixed-conifer systems in California, fire suppression policies have led to large, uncommon, fuel build and increased density. Fuel build-up and density contribute to high-severity crown fires that were historically rare (Syphard et al. 2007).

## 2.2 Climate Change in Southern California

Climate change is expected to produce increased surface air temperatures in California (Li et al. 2014), increased precipitation volatility (Swain et al. 2018), and a different seasonality of Santa Ana winds (Guzman-Morales and Gershunov 2019). California has seen an estimated 1℃ increase in temperature and an estimated 30% decrease in precipitation over the last 4 decades (Keeley et al. 2021). Since the 1970s, VPD has increased by 25% on burnable lands where vegetation is abundant

and ignitions are not limiting, warm-season days warmed by approximately 1.4℃ as part of a centennial warming trend, which has significantly increased the atmospheric vapor pressure deficit and will continue to into the future (Williams et al. 2019, Blach et al. 2022). As the climate warms, species compositions and productivity may change as higher temperatures affect growing seasons and temperature-driven changes to evapotranspiration affect the moisture needed for growth (Westerling 2016).

Ten-year projections indicate California summers are likely to become warmer and longer, with increased variability in precipitation (Swain et al. 2018) and little change in the mean (Li et al. 2014). Regional coupled ocean-atmosphere models predict an increase of around 2℃ along the coastal ocean area that increases progressively inland with anomalies of over 4℃ in summer (Li et al. 2014) Increased air temperatures will actively lower fuel moisture levels as warmer temperatures increase evapotranspiration as the ability for the atmosphere to hold moisture increases with higher temperatures (Flannigan et al. 2016).

The projected changes within a coupled model show an estimated summer precipitation increase of 0.11 mm/day (Li et al. 2014) Though a marginal increase in precipitation is predicted it is unlikely to compensate for increased summer temperatures lowering fuels moisture through escalated evapotranspiration. California is expected to have 6-14 fewer rainy days per year while projections suggest daily precipitation will increase in intensity it is unknown whether an increased intensity will offset the drying effects of fewer rainy days (Pierece et al. 2013). During the winter months, it is projected that southern California will see less

rain (~ -0.4 - -1.5 mm/day) (Li et al. 2014). Through the CESM-LENS ensemble, southern California is predicted to have a ~0% change in precipitation means (Swain et al. 2018), but an increase in precipitation variance of up to 50% (Swain et al. 2018).

Santa Ana winds (SAWs) are to change in the latter half of the century with a gradual decrease in early fall and late spring along with southern California experiencing a weaker offshore breeze (Li et al. 2014). Santa Ana winds occur when air from a high-pressure region over the southwestern United States flows westward towards the low-pressure zones located off the California coast. The peak of Santa Ana wind fires season in southern California occurs during the fall enabling the dry, cold, winds to fan some of California's greatest fires (Guzman-Morales and Gershunov 2019). A decrease Santa Ana winds in activity will be least pronounced during the winter peak of the Santa Ana wind season (Guzman-Morales and Gershunov 2019). While the strength of winds is expected to decrease, the frequency of Santa Ana winds will be more noticeable with the strongest being a 68% and 30% decrease in winds through September and October during the second half of the century. For the late winds, a forecasted decline in frequency of 35% in April and 50% in May for the latter half of the 21$^{st}$ century (Guzman-Morales and Gershunov 2019).

### 2.2.1 Projected Fire Regimes

Since the beginning of the Holocene, there has been a correlation between a changing environment and fire regimes (Keeley and Syphard 2016). Fire spread and

ignition probability are increased with lower moisture content within living or dead biomass. As droughts worsen, fuel moisture can be expected to decline accordingly. Years of high rainfall followed by drought years increase the variability of fire severity due to the increase in understory growth and eventual die-off. This variability in precipitation affects fire ignition and spread in ponderosa and shrubland environments becoming difficult for fire managers to predict forest fuels and ignition risk. In the Western United States, Parks et al. (2016) built a statistical model of fire severity as a function of climate that showed a mix of fire severity during the mid-21$^{st}$ century where cooler and/or wetter regions may experience higher severity levels with climate variability. Large portions of the west will likely experience decreased fire severity outside of those wetter regions (Parks et al. 2016). The probability of very large fire events defined as greater or equal to 23,234 hectares is suspected to increase by at least 30% projected through climate models for representative concentration pathway RCP4.5 and 8.5 with more days and months of extreme fire weather conditions of hot and moisture limited weather (Stavros et al. 2014).

Variability in the vapor pressure deficit (VPD) is the difference between the water vapor pressure at saturation and the actual water vapor pressure at a given temperature (Yuan et al. 2019) also changes. This is important as vapor pressure deficit provides one of the most important predictors of actual fire spread rate as an absolute measure of the difference between the air's water vapor content and its saturation value (Balch et al. 2022). VPD is also a strong predictor of fuel moisture, especially impacting fine fuels like leaf litter and small-diameter wood debris (Balch et al. 2022). A trend of increasing vapor pressure deficit values has been directly

connected to observed increases in burned area in Alaska's boreal forests and the western United States as a whole (Balch et al. 2022) indicating the response of summer forest-fire area to VPD is exponential. This relationship accounts for the fivefold increase in annual burned area within California from 1972-2018 (Williams et al. 2019). This trend of the daily minimum VPD increasing has the power to drastically increase the intensity of future fires through the creation of very low moisture environments and increasing the ability of fire spread.

Ponderosa and chaparral environments both share increased risks of fire ignition and spread based on herbaceous fuels increasing in density following years of high rainfall (Keeley and Syphard 2016). All fires thrive off a low moisture environment, but this does not always correlate to precipitation values. Within conifer forests, prior precipitation does not contribute to fire frequency as ignition ability and spread are largely dependent upon forest litter (Keeley and Syphard 2016). While rainfall might not be the large contributing factor to mixed conifer forests ignitions, it does play a part in ponderosa environments because of the more open nature of ponderosa systems, where understory growth and fuel loads are impacted by precipitation levels. Fuel-limited chaparral and shrubland ecosystems of southern California may experience reduced fuel abundance as a warmer climate reduces the growth of water-limited plants (Stavros et al. 2014). This effect may reduce the chance of very large fire events of ~23,234 hectares in chaparral systems.

### 2.2.2 Projected Vegetation Community Response

The climate changes described in section 2.2 will affect many vegetation communities in southern California. Despite a native vegetation community that is well adapted for California environments, the trend of increased temperatures, increased variability in precipitation, raising VPD, changing Santa Ana wind frequency, and the increased likelihood of longer droughts may stress and, in many cases, alter native environments (Kelly and Goulden 2008, Sykes 2009).

An increase in vapor pressure deficit negatively affects vegetative communities' photosynthetic rates through stomatal closure, reducing plant carbon uptake, which is a larger influence on plant productivity than changes in precipitation (Konings et al. 2017). VPD reduces vegetation growth (Konings et al. 2017) and is a primary driver of drought-stress within forest systems (Williams et al. 2012). Soil moisture will continue to decrease through evapotranspiration as spring and summer VPD increases (Williams et al. 2012). VPD has been projected to steadily increase well into 2100 (Yuan et al. 2019), hindering vegetative communities' ability to operate as a carbon sink.

The expected effects changes in Santa Ana winds will be a more condensed fire season in southern California. Traditionally the peak of wildfire season is October, but this peak may change to November-December creating a shorter fall and winter fire season. This more tapered Santa Ana winds season could possibly result in less frequent large fires during fall and winter as Santa Ana winds tend to become the main driver of large wildfires during those months (Guzman-Morales

and Gershunov 2019). It must be considered that this shorter season will likely follow an even drier summer with winter precipitation forecasted and thus may not make up for the summer decrease in precipitation at the tail end of the 21st century.

California's native biodiversity has become threatened and changing climate conditions will further promote the spread of non-native species through native shrublands and grasslands (Sandel and Dangermond 2011). California's year-to-year unpredictability of precipitation patterns and projected increase in dry days (Polade et al. 2014) will heavily influence California vegetation, particularly endemics. Endemic species in California are in decline. Climate modeling by Battle et al. (2008) in southern Californian forests shows a link between increased temperatures and stem volume growth declines due to less moisture and a shorter growing season due to heightened surface air temperatures. Within Californian forests, stress induced by the increased variability of rain will invite pests, such as bark beetles, and pathogens to attack weakened trees, leading to increased mortality (Safford and Stevens 2017). A year of increased precipitation followed by a year of intense drought will result in a dense environment of low-moisture grassland fuels ready for conflagration via SAWs. Large fires are historically apart of chaparral shrublands in California and burn in stand-replacing fires throughout the California Floristic Province (Franklin 2009) and low-to-moderate intensity fires are a historical norm in mixed conifers. fire exclusion through forest fire suppression policy and increased fire frequency in chaparral have altered vegetation dynamics in these systems. In a study by Janet Franklin (2009) vegetation from 38 stands was surveyed examining plant invasion following fire. Stand-replacing fires led to shrub

cover increase from 3-to-31%, exotic herbaceous cover from 3-to-40%, and native annuals dropped from 33-to-15% (Franklin 2009) benefiting non-native species. As development continues along wildland-urban interface and intermix areas, where houses and vegetation directly intermingle, the interactions between human activities and vegetation alter fire regimes and can lead to species displacement (Syphard et al. 2007).

## 2.3 Wildland-Urban Interface

The wildland-urban interface (WUI) is the area where houses and undeveloped wildland vegetation meet and intermingle, it is an area where wildfire problems are become more pronounced (Radeloff et al. 2018). WUI is defined by the *Federal* Register as areas with a housing density greater than 6.17 houses per $km^2$ and vegetation cover >50%. The percentage of vegetation cover is derived through extracting land cover data from the National Land Cover Database within each census block where >50% is intermix and >75% vegetation cover is interface zones (Glickman & Babbitt 2001). WUI expansion in the United States has grown rapidly between 1990 to 2010 with an increase from 30.8 to 43.4 million homes and WUI classified land areas from 581,000 to 770,000 km2 (Radeloff et al. 2018). Suburban development within the WUI creates threats to vegetation as the development of these areas introduces habitation loss and fragmentation leading to lower levels of biodiversity (Radeloff et al. 2005). In California there are 4.5 million homes within the WUI, requiring the use of different fire suppression tactics at increased cost compared to remote fires (Schoennagel et al. 2017). Even with the WUI holding one-

tenth of the land area in the conterminous United States 43% of all new homes were built there (Radeloff et al. 2018).

In southern California when urbanization reaches undeveloped foothills and canyons, these areas become highly profitable, but risky, for suburban housing (Garrison and Huxman 2020). Further development of vegetated areas into low-density housing increases the likelihood of fire activity as wildfires do not share a correlation to where the population is highest (Syphard et al. 2019). Home construction in the WUI increases the risk of wildfires occurring all while increasing fuel loads through structures and fire-prone landscaping (Garrison and Huxman 2020). If these developments experience fire insurance policies, state and federal subsidies, and disaster recovery funds shield homeowners from paying the full price of protecting their risky investments (Garrison and Huxman 2020). These policies could reinforce the continual development of the WUI. The trend of wildfires becoming larger is accelerating in California, this is seen in the WUI as well increasing total structure damage over the past four decades where average annual loss grew from $0.03 billion between 1979-1988 to almost $1 billion between 2009-2018 (Buechi et al. 2021). Increased urbanization of southern California is creating expanded WUI area where larger parts of the population may be put at risk. In the western United States 3.6 million hectares are set to be exposed to moderate to large increases in wildfire risk in the next twenty years (Schoennagel et al. 2017).

The future of how fire and WUI expansion will interact with one another to the mid-21st century and beyond has not been covered in detail. Modelling has been done to understand different aspects of fire-WUI relationships in the western United

States Safford, Schmidt, and Carlson 2009 had the opportunity to assess how fuel treatments effecting wildfire severity in the WUI in response to the Angora Fire, which burned into 194 ha of fuel treatments. They found that fuel treatments can modify fire behavior and change crown fire to surface fires within 50 meters of encountering a fuel treatment (Safford, Schmidt, and Carlson 2009). Work by Syphard et al. 2019 modelled the importance of climate and human variables to explain fire patterns and structure loss across three regions in California. Their work suggested urban areas contributed more to fire ignitions and structure loss while climate and other geographic variables were important explanatory variables to a fire's ability to reach larger sizes (Syphard et al. 2019). Work has also been done using LANDIS-II to explore interactions of wildfire, succession, and fuels management over 50 years in the southern Sierra Nevada, California on a landscape of $2.2 \times 10^6$ hectares in size and examine how fires responded to fuels treatment (Syphard et al. 2011).

While work has been done to understand the relationship between fire and fuel treatment (Syphard et al. 2011), how fire responds to fuel treatment in WUI areas (Safford, Schmidt, and Carlson 2009), and how important climate and human infrastructure is in modelling structure loss in California (Syphard et al. 2019), there remains gap in an understanding of how future fire projections may interact with potential future California urban development. It is important to understand the conceivable risks of fire intersecting with expanding development as structure loss in southern California is significantly correlated with low-to-medium density housing (Syphard et al. 2019).

## 2.4 Landscape ecology models

Landscape models (Wiens & Milne 1989, Forman & Godron 1981, Steele 1989) have been in development since the late 1980s and are used from the scale small habitats to regional simulations. The broad scales found in early landscape ecology modelling found that there are limits on what could be understood empirically across dynamic spaces leading to a need for spatial models which can use stochastic elements to conduct experiments through simulations. As the development of landscape ecology modelling became more advanced and computing power increased, there became more advanced ecological questions that empirical models could not address, leading to stochastic models or simulators (Mladenoff 2004).

Spatial models can simulate entities through cells that have coordinates, but these models are not always spatially dynamic, meaning they include explicit locations of what is being studied, but also processes that create interactions amongst the studied landscape that drive change over various time-steps. The stochasticity of these models and ability to simulate multiple replicates generates trajectories of system change thought of as a simulated version of the natural range of variability (Mladenoff 2004). Empirical and analytical models are constrained to answer limited questions, while spatially dynamic models like LANDIS can simulate possible futures being able to analyze landscape changes through stochastic ecosystem simulations. Landscape models are constrained by their extent and the degree to which the model incorporates mechanistic detail and spatial dynamics,

and cell size (Mladenoff 2004). LANDIS uses rasters due to several advantages, that they are both being the faster than vector in general and, if incorporated into the design, being capable of representing the greatest range of the resolution/extent space (Mladenoff 2004)

The goal of LANDIS, which is an abbreviation of 'landscape disturbance and succession', was to simulate large forest landscapes (100 s ha – 1000 s $km^2$) with inclusions of succession, wind, and fire disturbances that operate spatially (Mladenoff 2004). LANDIS and LANDIS-II are raster map-based models that operate on interactive cells providing a mechanistic detail that is broad enough to be well suited over many different landscapes (Mladenoff 2004). The introduction of a shift in philosophy from LANDIS centralized model development to a decentralized LANDIS-II extension development and moving to variable timesteps creates a model that can model various forest landscape effects where disturbance frequency is high or successional processes long (Scheller et al. 2007).

### 2.4.1 Modeling Vegetation Succession Dynamics with LANDIS-II

LANDIS-II is a forest landscape model that can simulate vegetation, including forests, shrublands, and grasses. The model can simulate change through a function of growth and succession influenced by different disturbances. LANDIS-II has been used to model a variety of ecosystem processes such as modeling and forecasting forest evolution (Ciceu et al. 2020), modeling potential effects of current biodiversity approaches on future habitation modification under diverging climate scenarios (Mairota et al. 2013), and modeling how ungulates can alter forest productivity and

vegetation succession (De Jager et al. 2017). Furthermore, LANDIS-I has been used with the Clark Urban Growth Model to simulate the effects of urban development and high fire frequency on the distribution of coastal shrublands (Syphard et al. 2007). LANDIS capability to be highly customizable, one can model vegetation succession and the different dynamics that take place across a varied landscape.

LANDIS - II emphasizes species life history attributes of longevity, shade tolerance, fire tolerance, and dispersal ability, amongst others to drive succession and disturbance over the extent (Scheller et al. 2007). Species are modelled individually as species-age cohorts where multiple species can occupy the same space allowing species to respond differently to varying environmental drivers (Scheller et al. 2007). Each unique species has its own range of ideal temperatures and moisture ranges, making every species respond differently to climatic projections (Maxwell et al. 2022).

To simulate forest succession the Net Ecosystem Carbon and Nitrogen (NECN) (Scheller et al. 2022) growth extension was selected for the model. NECN was selected as it is an expansion upon the CENTURY model (Parton 1996) succession extension that was built into the LANDIS framework that has been used prominently (Krofcheck et al. 2017). The expansion of the CENTURY model LANDIS extension into NECN included regeneration function for species that can experience regeneration (Erikson & Strigul 2019). The purpose of NECN is to estimate ecosystem carbon and nitrogen between living and dead matter, and soil pools following the CENTURY model (Parton 1996). NECN can calculate how cohorts grow, reproduce, age, and die (Krofcheck et al. 2017). Upon death, biomass can be

tracked into different pools of surface litter, soil litter, soil wood, and surface wood. Being able to account for nitrogen is important when it comes to modelling the effects of frequent fire in native coastal shrub environments where increased nitrogen deposition rates and strain from urban conversion may increase loss within scrub communities (Talluto and Suding 2008). As anthropogenic warming continues to affect vegetative species and changing fire regimes, coupled with increased high-severity fire risk from fire exclusion policies, could destabilize forest carbon and reduce the ability of forests to regulate climate through carbon sequestration (Krofcheck et al. 2017).

### 2.4.2 Modeling Fire Dynamics with LANDIS-II

We chose LANDIS-II to capture the amount of variability increases within human policies regarding fire, vegetation response, climate, and fire itself over time. Within the LANDIS-II framework, Social-Climate Related Pyrogenic Processes and their Landscape Effects (SCRPPLE) extension (Scheller et al. 2019) gives the ability to simulate these interactions and changes.

Unlike stand-alone fire models, landscape simulation models can integrate human actions, fire, and vegetation, amongst other drivers of landscape disturbances and vegetation succession. SCRPPLE's development has put attention on the social dimensions of fire through human ignitions, spatial and temporal patterns of prescribed fire, fuel treatment effects, and spatial patterns of fire suppression. Considering the model's focus on the greater determinants of fire behavior, SCRPPLE produces an array of outputs portraying information about fire

regimes, including predicted wildfire ignitions, fire intensity and spread, annual ignitions, burn frequency, simulated fire size distributions, hectares burned, and vegetation mortality.

Fire behavior models are highly capable of modeling ignition, fire spread, and at landscape scales which can interact with vegetation patterns, fuel, topography, and weather, they are lacking in the ability to incorporate vegetation change or feedback from human activities, vegetation, climate, and fire over time (Scheller et al. 2019). Modern fire regimes have largely become a product of human interactions with their environment. For some time now there has been a range of fire models designed for different purposes. Fire spread has been modeled through cellular automata models, empirical and semi-empirical fire behavior, and spread models calibrated through field data, or physics-based combustion spread models (Scheller et al. 2019). The ability to dynamically map fire is of great importance as models such as LANDSUM (Keane et al. 2006) or ALFRESCO (Rupp et al. 2000) are only spatially explicit when it comes to fire. SCRPPLE is spatially interactive, meaning each cell interacts with another, which allows fire to spread across the landscape.

Capturing these dynamics is crucial to understanding of future fire in southern California from a modelling perspective. There is a gap in research that this work could alleviate. LANDIS-II has been used in southern California (Syphard et al. 2007, Krofcheck et al. 2017) and SCRRPLE has been used to analyze fire regimes in the Lake Tahoe Basin (Scheller et al. 2019) but modelling how future fires may impact projected urban development has not been done. Being able to assess potential fire frequency and severity projections for the future of this region under

different climatic projections will give a greater understanding of plausible risks intersecting urban growth. Through a combination of knowledge, it has been possible to parameterize LANDIS-II with an understanding of vegetation, climate, and fire dynamics to efficiently assess fire risk through different climatic lenses. Filling in a gap in the current literature will impart the ability to know how often fires occur in current WUI areas and how often wildfires intersect the WUI and planned future southern California development to the year 2100.

## 3.0 Methods

To understand these complex relationships between fire, climate, and vegetation, the model LANDIS-II, a landscape change model, was applied to discern how projected fire will interact with future urban growth in southern California to the year 2100.

## 3.1 Study Area

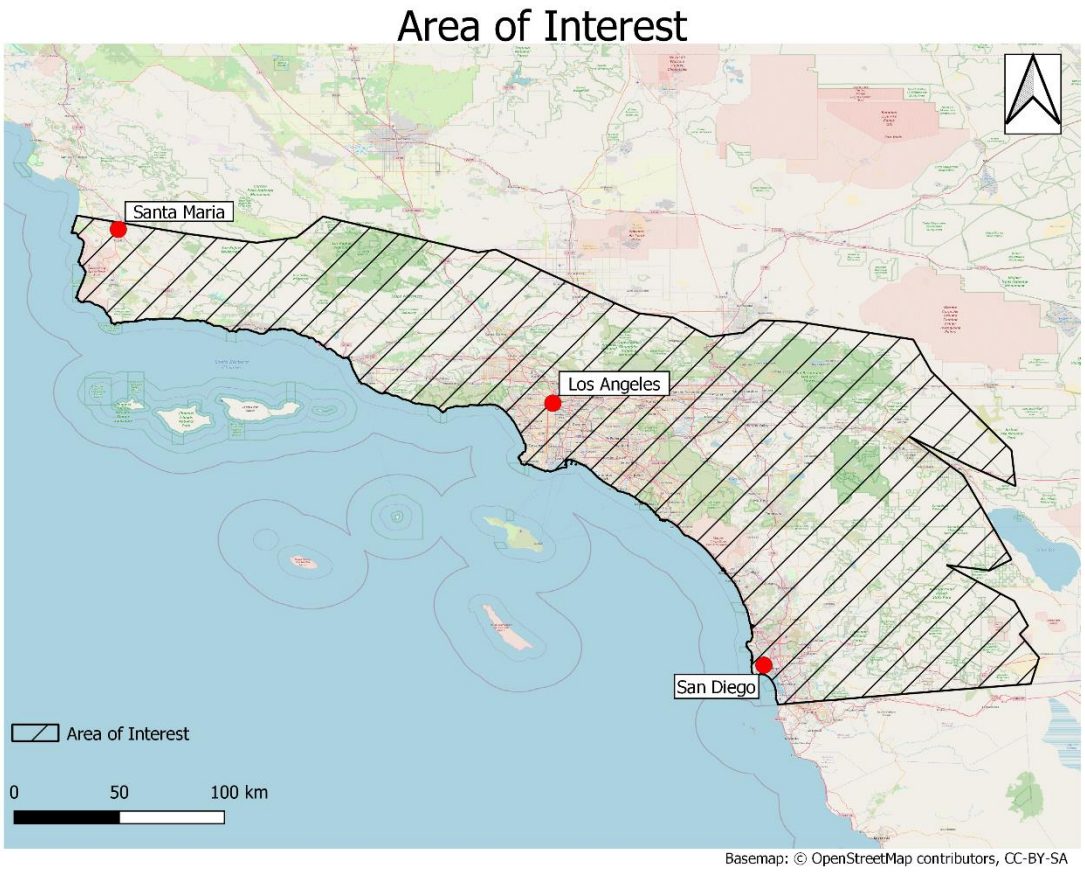


Fig. 1 – Area of Interest in southern California a size of 4,816,319 hectares

The area of interest (Fig. 1) was chosen as southern California holds important biodiverse ecosystems that, with rapid global change, have shifted fire regimes and can disrupt ecological function causing ecological services loss (Syphard et al. 2022). The study area comprises a large portion of southern California's Mediterranean-type ecosystems characterized by mild wet winters and warm dry summers. The study area is a part of the California Floristic Province (CFP) is an area of high biodiversity and endemism which has been aided by the

geo-climatic setting of the region where 6,927 species are native to CFP with 2,612 vascular plants being endemic to the area (Burge et al. 2016).

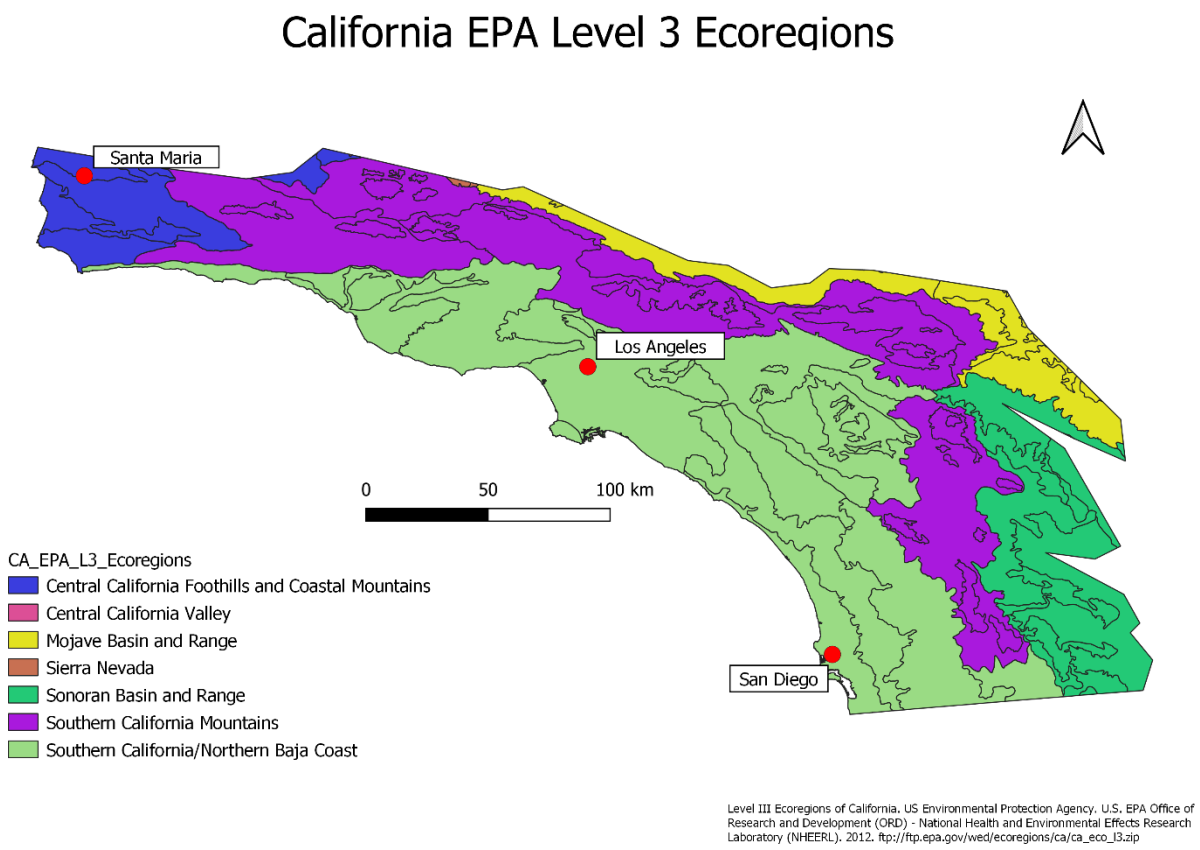


Fig. 2 – California Level III EPA ecoregions over the study area

The study area consists of various ecoregions described by the United States Geological Survey (Omernik 1987) shown in figure 2. In the north-west of the area of interest the Central California Foothills and Coastal Mountains (CCFCM) have the characteristics of hot dry summers and cool moist winters primarily associated with chaparral and oak woodlands, with grasslands at low elevations with small patches of pines at high elevations. To the south of the CCFCM is the Southern California/Northern Baja Coast (SCNBJ) an area of alluvial plains, marine terraces,

and low hills of southern California where coastal sage scrub and chaparral are widespread. These low hills also include various oak species leading to the Santa Monica and Santa Ana Mountains where some firs and pines inhabit the high range. To the east and north of the SCNBJ are the Southern California Mountains (SCM) with the ranges of the Sana Ynez, Sierra Madre, San Rafael, San Gabriel, San Bernadino, and San Jacinto mountains domination this region characterized by hot dry summers and moist cool winters. The SCM ranges have higher elevations with cooler temperatures and more precipitation than other regions leading to denser vegetation. The Transverse Ranges in this region (all the ranges listed besides Santa Jacinto) receive 30-40 inches precipitation a year on the south-facing slope and 15-20 on the northern slope. High evaporation rates on the south-facing slopes contribute to more chaparral growth and the slower evaporation and lower annual temperatures on the northern slope encourage coniferous forests that dissipate to desert montane as it approaches the Mojave. The Mojave Basin and Range is warmer and drier than the aforementioned regions with the primary vegetative bodies being cactus and shrubs. The final major EPA region in the study area is the Sonoran Basin and Range, which is similar to the Mojave with scattered low mountains and containing shrubs and cactus (Griffith et al. 2016).

This region of southern California is home to millions of people and some of the most dynamic fire conditions on the planet. Along with the prospect of global change, a biodiverse region, and rapidly expanding human settlement makes this a critical environment in which to understand the state of future forests, and subsequently, wildfire conditions.

## 4.0 Modeling with LANDIS – II

Under the LANDIS–II framework, climate and environmental interactions of tracking carbon sequestration, nitrogen limits, and nitrogen deposition were simulated to estimate forest conditions and enable parameterization of wildfire models in 2050 and 2100. The following sections have been organized to explain the parameterization of LANDIS - II NECN (Net Ecosystem Carbon and Nitrogen) succession extension. Each section describes the data sources used and pre-processing applied to parametrize the model.

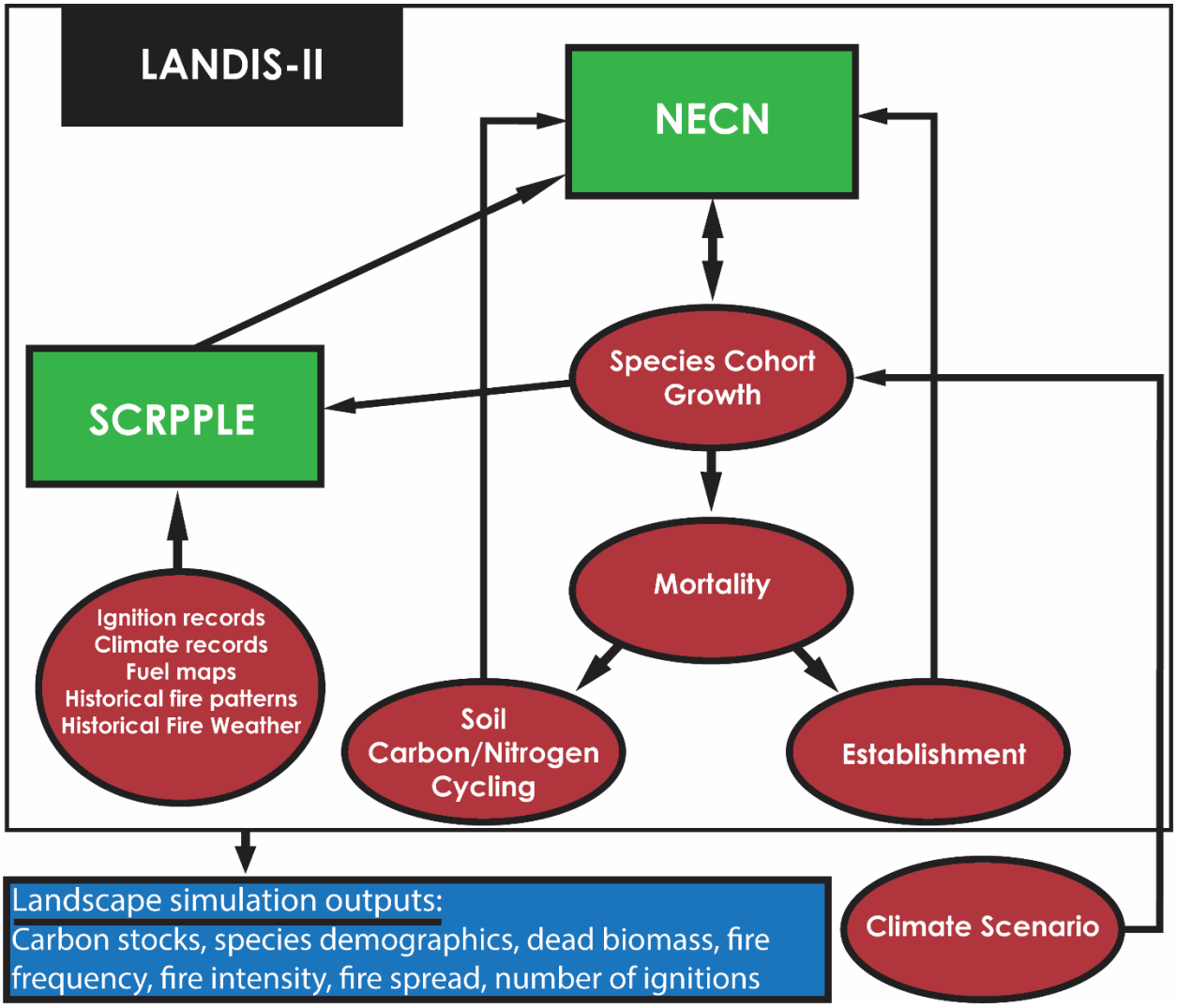


Fig. 3 – The green boxes represent extensions used within the LANDIS-II model core. The red ovals represent data with directional arrows showing generalized interactions with the extensions. The blue box shows the outputs that can be received. NECN incorporates the influence of temperature, water, nitrogen, and light-based competition to determine species growth and regeneration where SCRPPLE simulates the probability of fire, spread, and mortality (Robbins et al. 2022).

LANDIS views the landscape as a grid of connected cells simulating vegetation and disturbances between andwithin cells as a continuous landscape. The Net Ecosystem Carbon and Nitrogen (NECN) succession extension of LANDIS-II incorporates temperature, water, nitrogen, and competition for light to determine species vigor and regeneration. SCRPPLE simulates the probability of fire, spread,

and mortality across the landscape on a daily basis based upon climate, topography, vegetation, and fine fuels.

## 4.1 NECN Model Inputs

Table 1 –NECN model inputs.

| NECN Input | Data Needed | Data Type | Data Source |
|---|---|---|---|
| Soil properties (pg 36) | See Table 2 | See Table 4 | SSURGO (Soil Survey Staff 2022), soil carbon estimates created by West, T.O. (2014), Forest Inventory and Analysis data (Gray et al. 2012) |
| Ecoregions (pg 31) | Annual max/min temperature, annual max/min precipitation, annual max/min vapor pressure deficit | CSVs | PRISM Climate Group, Oregon State University, https://prism.oregonstate.edu, data created 4 Feb 2014, accessed 11 Nov 2021. |
| Climate (pg 35) | Projected climate and historical climate with mean, variance, and standard deviation of precipitation, max temperature, and min temperature | CSVs | USGS geodata portal Multivariate Adaptive Constructed Analogs (MACA) CMIP5 Statistically Downscaled Data for Coterminous USA (Blodgett et al. 2011) |
| Initial Communities (pg 42) | age and biomass of vegetative cohorts and map of communities | Text file and associated raster | Map of communities (Riley et al. 2019, Comer et al. 2003), biomass and carbon from FIA (Gray et al. 2012), ages for Mountain-Mahogany (475) (Brotherson et al. 1980), ages for Pinyon species (106, 133, 134, 140, 141, 143) (Gascho Landis and Baily 2006), ages for California Laurel (981) (Barry 2014), other species in house age equation was applied based on height and site index. |
| NECN_Functional_Table, NECN_Spp_Table (pg 51) | Species life parameters | CSVs | (Lucash et al. 2017, Liang et al. 2016, Huang et al. 2020, Scheller et al. 2011, Syphard et al. 2011, Spencer et al. 2011), (Abrahamson 2014) |

| | | | |
|---|---|---|---|
| NECN species properties (pg 33) | Species life parameters | Text file | (Lucash et al. 2017, Liang et al. 2016, Huang et al. 2020, Scheller et al. 2011, Syphard et al. 2011, Spencer et al. 2011), (Abrahamson 2014) |

For the soil input maps, all rasters have been set to 100m resolution; all rasters need to have the same resolution and extent.

Table 2 – Table describing the soil inputs and where the data was originally sourced from along with providing the data type needed for the raster maps.

| Soil Map | Data Type | Data Source |
|---|---|---|
| SoilDepthMapName | Float | SSURGO (Soil Survey Staff 2022) |
| SoilDrainMapName | Float | SSURGO (Soil Survey Staff 2022) |
| SoilBaseFlowMapName | Float | Following Bisquay 2021 and Robbins et al. 2022, BaseFlow set to .01 |
| SoilStormFlowMapName | Float | Following Bisquay 2021 and Robbins et al. 2022, BaseFlow set to .01 |
| SoilFieldCapacityMapName | Float | SSURGO (Soil Survey Staff 2022) |
| SoilWiltingPointMapName | Float | Following Bisquay 2021, WiltingPoint was calculated by dividing FieldCap by two |
| SoilPercentSandMapName | Float | SSURGO (Soil Survey Staff 2022) |
| SoilPercentClayMapName | Float | Calculated based on (West, T.O. 2014) |
| InitialSOM1CsurfMapName | Float | Calculated based on (West, T.O. 2014)) |
| InitialSOM1NsurfMapName | Float | Calculated based on (West, T.O. 2014)) |
| InitialSOM1CsoilMapName | Float | Calculated based on (West, T.O. 2014) |
| InitialSOM1NsoilMapName | Float | Calculated based on (West, T.O. 2014) |
| InitialSOM2CMapName | Float | Calculated based on (West, T.O. 2014) |
| InitialSOM2NMapName | Float | Calculated based on (West, T.O. 2014) |
| InitialSOM3CMapName | Float | Calculated based on (West, T.O. 2014) |
| InitialSOM3NMapName | Float | Calculated based on (West, T.O. 2014) |
| InitialDeadWoodSurfaceMapName | Float | FIA (Gray et al. 2012) |
| InitialDeadCoarseRootsMapName | Float | FIA (Gray et al. 2012) |

| | | |
|---|---|---|
| Ecoregions/Climate_Regions | int32 | Calculated based on PRISM Climate Group, Oregon State University, https://prism.oregonstate.edu, data created 4 Feb 2014, accessed 11 Nov 2021. |
| Initial_Communties(IC_MAP) | int32 | Map of communities (Riley et al. 2019, Comer et al. 2003) |

### 4.1.1 Ecoregion/Climate Regions

LANDIS – II NECN uses ecoregions or climate regions to describe areas for climate data. NECN uses climate regions through the NECN-succession-log, a file that outputs a snapshot of data at every successional time step. These data are averaged by climate region and are most useful for analyzing variation over time and across climate regions (Scheller et al. 2022). Climate regions are further used in the NECN-prob-establish-log output file containing the data used to calculate the probability of seeding establishment for each climate region at each succession time step (Scheller et al. 2022).

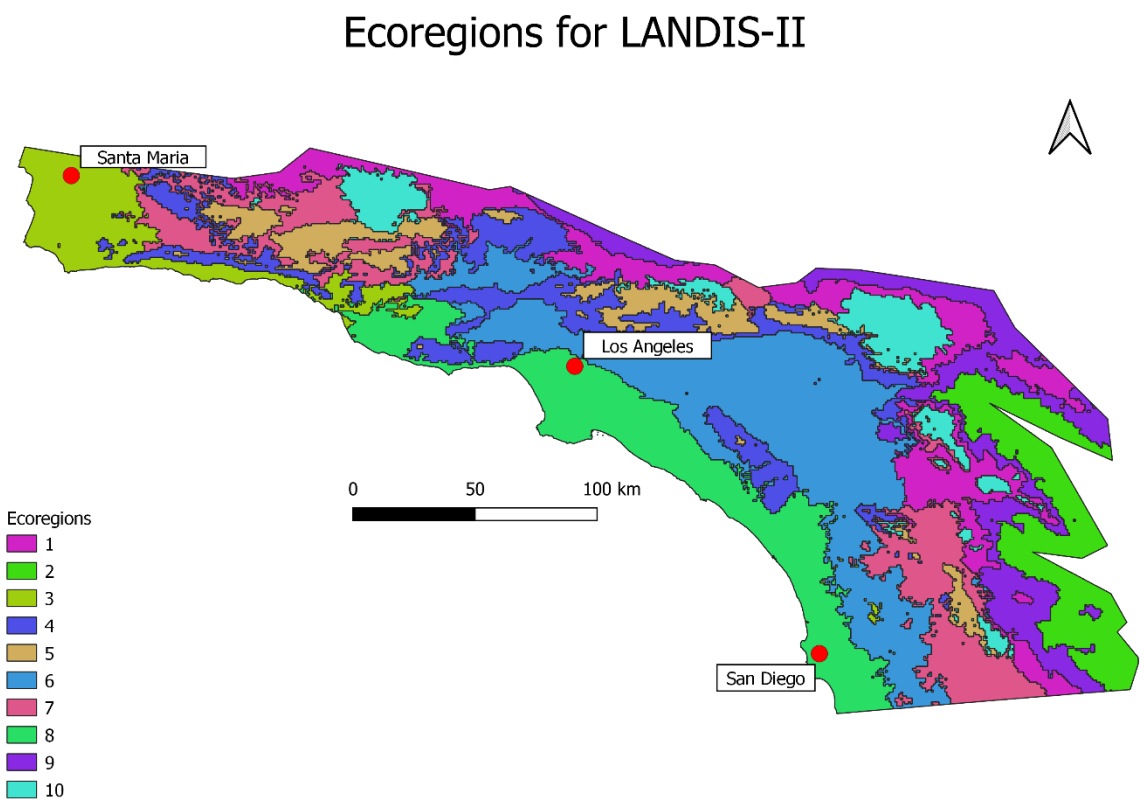


Fig. 4 – Study area ecoregions found for LANDIS – II

Table 2 – Zonal statistics describing different means of climate variables from study area ecoregions.

| Ecoregion | VPDmin_mean(hPa) | VPDmax_mean(hPa) | Tmin_mean(c) | Tmax_mean(c) | PPT_mean(mm) | PPTmin_mean(mm) | PPTmax_mean(mm) | DEM_min(m) | DEM_max(m) |
|---|---|---|---|---|---|---|---|---|---|
| 1 | 13 | 23.16 | 7.88 | 22.19 | 328.44 | 177.38 | 760.09 | 444.91 | 2235.49 |
| 2 | 31.08 | 37.03 | 14.39 | 30.06 | 102.25 | 62.28 | 340.9 | -70.28 | 1048.94 |
| 3 | 17.45 | 23.47 | 7.25 | 23.17 | 532.43 | 250.85 | 1176.84 | 132.88 | 1992.99 |
| 4 | 14.11 | 21.58 | 10.73 | 23.14 | 582.91 | 355.58 | 950.42 | 44.22 | 1801.55 |
| 5 | 12.35 | 18.51 | 7.53 | 19.64 | 828.55 | 430.84 | 1327.64 | 343.26 | 2817.95 |
| 6 | 16.55 | 23.76 | 10.65 | 25.39 | 380.2 | 213.8 | 634.84 | 48.24 | 1277.53 |
| 7 | 7.59 | 15.34 | 12.26 | 22.66 | 345.68 | 227.31 | 632.45 | -4.85 | 778 |
| 8 | 23.46 | 30.24 | 10.28 | 25.92 | 204.62 | 105.04 | 457.79 | 209.26 | 1550.42 |
| 9 | 9.87 | 17.15 | 3.39 | 17.46 | 568.11 | 218.2 | 1410.3 | 1006.87 | 3500.06 |
| 10 | 5.79 | 14.59 | 9.42 | 21.29 | 460.08 | 322.22 | 714.57 | 0 | 1081.13 |

To obtain ecoregions, a form of k-means clustering analysis was applied to vapor pressure deficit, temperature, and precipitation climatic variables to identify clusters. The goal of climate regions, or ecoregions, within NECN is to assign homogenous climate projections across different regions. With this method, clusters

were found within the data in such a way that the sum of the squared distances between the data points and the centroid is as small as possible making likewise groups. A k-means algorithm clusters data by trying to separate samples in *n* groups of equal variance, minimizing *inertia*, a measure of how internally coherent clusters are, this method scales well over a large number of samples working well within a large area of interest. A disadvantage of K-means algorithm is its sensitivity to the initialization of centroids or the mean of points. Errors where one centroid is initialized as a “far-off” point may end up with no points associated with it or more than one cluster may be linked with a single centroid. To overcome this method K-means++ is used for the study. K-means++ ensures a smarter initialization of centroids improving the quality of clustering.

To prepare the climate data, a geodataframe was created through the geopandas Python library dropping Nans (rows where there is no data available), creating points from latitude and longitude, then joining each of the climate variables based on Shapely, a Python package for set-theoretic analysis and manipulation of planar features, geometry to obtain a dataframe on which the clustering could be completed. The data is then normalized using the Python package scikit-learn’s StandardScalar standardizing features by removing the mean and scaling to unit variance. It is important to normalize the climate variables to ensure that the distance measure accords equal weight to each variable to prevent the variable with the largest scale dominating the clustering pattern ensuring each feature makes an equal contribution (Singh and Singh 2020).

Figure 4 shows the LANDIS-II ecoregions within the area of study which is three more regions than the level 3 EPA California Ecoregions. K-means clustering was used to identify ecoregions which found that 10 ecoregions was the point where anything after found the diminishing returns where the cost of subsequent centroids no longer increase the benefit of minimizing the distance one centroid to another (Yock and Kim 2017, Kanungo et al. 2002). Table 2 shows the varied climatic and physical variables found across the study area. This table shows the variation between the regions with mean low precipitation across the regions. It is important to note that while EPA Ecoregions include vegetation, human settlements, soil, air, and water while LANDIS-II ecoregions only consider climatic variables. The ecoregion shapes for LANDIS-II are built off only climate variables which are fed to a repository of climate data (Lucash et al. 2017) that perform climate projections based on these homogenous regions.

To find the ideal number of clusters k-means clustering with elbow was used shown in figure 4. The elbow Method is a heuristic used in determining the number of clusters in a data set, was employed (Marutho et al. 2018). The elbow method can be used to optimize the number of clusters with k-means clustering method finding the point where improvement in distortion of *k* declines the most which determines when to halt the dividing of clusters. The max number of clusters was set to be 15 the elbow method found the knee of the curve to be 10 clusters.

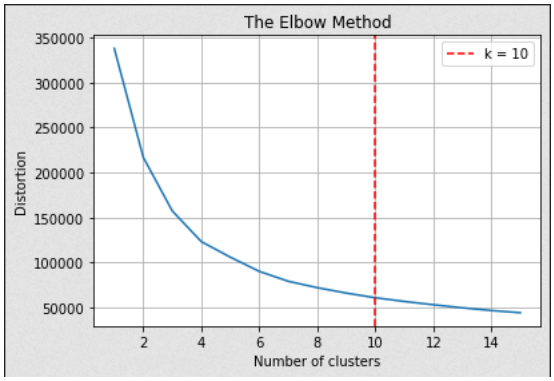


Fig. 5 – Showing the fit of *k* number of clusters found through the k-means++ to the climate data used in creating climate region.

The output of the k-means++ was a point file that was then polygonized to obtain the polygons shown in figure 2. The polygons were then rasterized for input into LANDIS-II NECN.

## 4.1.2 Climate Data

Climate in NECN is built around a central climate library made for LANDIS-II (Lucash et al. 2017). Climate data for LANDIS-II NECN is aggregated to the climate unit of 'climate regions.' The climate regions shapefile is used as the areal unit in which to aggregate climate data. A compressed (*.zip) shapefile was uploaded to the USGS GeoData Portal (Blodgett et al. 2011) to obtain climate data based on the 10 ecoregions. LANDIS-II ingests future and historical for daily precipitation, daily maximum, and minimum near-surface air temperature, max and minimum relative humidity, wind direction, and wind speed. These variables are static in the model and are read at each timestep allowing LANDIS-II to account for climate variability to produce realistic results of species composition, disturbance regimes, and ecosystem dynamics (Lucash et al. 2017).

Future climate projections for the three model runs were from 2019 to 2099. The first was CNRM-CM5.1 (Voldoire et al. 2013) which we characterized as the “Greater Precipitation” model having a mean average daily precipitation over 81 years across ten ecoregions of 1.5 mm. This model also experienced the lowest max temperature mean at 298.95 k. The second climate projection used was GFDL’s ESM2G (Dunne et al. 2012), where this data set is characterized as “Mean Precipitation” with the mean daily precipitation at 1.22 mm and the max temperature mean at 299.33 k. The third global climate model used was MIROC-ESM (Watanabe et al. 2011), characterized as “Less Precipitation” with a daily average mean of 1.01 mm and a maximum temperature mean of 299.99 k. This data is then read into the climate library that will perform all necessary pre-processing for all climate-dependent LANDIS-II extensions (Lucash & Scheller 2021). Historical data has the same variables but is from the University of Idaho, METDATA (Abatzoglou 2013), covering the years 2000-2018.

### 4.1.3 Soil

LANDIS – II NECN uses 18 different soil maps to simulate future landscapes. To create the NECN soil input soils data from the Soil Survey Geographic (SSURGO) (Soil Survey Staff 2022) containing vector and tabular information about different soil properties, deadwood data obtained from the US Forest Inventory and Analysis Program (Gray et al. 2012), and total carbon and nitrogen maps were calculated by using West, T.O. (2014) CONUS level carbon map.

Table 4 – Overview of what maps are needed for NECN and a short description of what the maps do. Each map has a superscript associated with it and those maps that share a superscript will be referenced, for example, as **Maps[1]** this is to denote that all the maps under superscript 1 share the same data source.

| Soil Maps | Data Source | Description |
|---|---|---|
| Soil Depth[1] | SSURGO (Soil Survey Staff 2022) | The depth of simulated soil. |
| Soil Drain[1] | SSURGO (Soil Survey Staff 2022) | Determines the amount of water runoff and leaching. The fraction of excess water lost by drainage. The soil drainage factor allows a soil to have differing degrees of wetness. |
| Field Capacity[1] | SSURGO (Soil Survey Staff 2022) | The amount of soil moisture or water content held in the soil after excess water has drained away |
| Wilting Point[1] | SSURGO (Soil Survey Staff 2022) | The minimum amount of water in the soil that the plant requires not to wilt. |
| Percent Sand[1] | SSURGO (Soil Survey Staff 2022) | Percentage of sand in the soil. |
| Percent Clay[1] | SSURGO (Soil Survey Staff 2022) | Percentage of clay in the soil. |
| SOM1surfC[2] | soil carbon estimates created by West, T.O. (2014) | The initial, timestep 0, amount of carbon in the soil surface. |
| SOM1surfN[2] | soil carbon estimates created by West, T.O. (2014) | The initial, timestep 0, amount of nitrogen in the soil surface. |
| SOM1soilC[2] | soil carbon estimates created by West, T.O. (2014) | The initial, timestep 0, amount of carbon in the soil sub-surface. |
| SOM1soilN[2] | soil carbon estimates created by West, T.O. (2014) | The initial, timestep 0, amount of nitrogen in the soil sub-surface. |
| SOM2C[2] | soil carbon estimates created by West, T.O. (2014) | The initial, timestep 0, amount of carbon in the ‘slow’ soil pool. |
| SOM2N[2] | soil carbon estimates created by West, T.O. (2014) | The initial, timestep 0, amount of nitrogen in the ‘slow’ soil pool. |
| SOM3C[2] | soil carbon estimates created by West, T.O. (2014) | The initial, timestep 0, amount of carbon in the ‘passive’ soil pool. |
| SOM3N[2] | soil carbon estimates created by West, T.O. (2014) | The initial, timestep 0, amount of nitrogen in the ‘passive’ soil pool. |

| | | |
|---|---|---|
| Dead Wood on the Surface[3] | Forest Inventory and Analysis data (Gray et al. 2012) | The initial, timestep 0, amount of surficial dead woody material. |
| Dead Wood of Coarse Roots[3] | Forest Inventory and Analysis data (Gray et al. 2012) | The initial, timestep 0, amount of belowground dead woody material. |
| Base Flow[4] | Stationary variable | Determines the amount of water runoff and leaching. The fraction per month of subsoil water going into stream flow. |
| Storm Flow[4] | Stationary variable | Determines the amount of water runoff and leaching. The fraction of the soil water content lost as fast stream flow. |

**Maps[1]** were obtained from USGS SSURGO California database (Soil Survey Staff 2020). SSURGO contains information about soil collected by the National Cooperative Soil Survey. SSURGO data uses a component and map key system, requiring attribute joins to create a map of a single trait. The four tables that were joined were the *chorizon*, *component*, *conmonth*, and *corestriction* tables.

The *chorizon* table, referred to as *Horizon*, lists the horizon(s) of various components of the soil. A horizon is a layer of mineral soil that has a defined soil structure. This table holds the attributes of *wfifteenbar_r*, which is the volumetric content of soil water retained at a tension of 15 bars. This attribute was used to obtain our wilting point. The wilting point within the model is the point when there is no water available to vegetation. *Wthirdbar_r* is the volumetric content of soil water retained at a tension of 1/3 bar. LANDIS-II NECN ingests this as a map of field capacity. Field capacity being the water remaining in soil after it has been saturated then allowed to drain. The *sandtotal_r* and *claytotal_r* are both mineral particles of 0.05mm to 2.00mm expressed as a percentage within the soil. Clay and sand are

both important components to vegetation growth, carbon or nitrogen can leach out of sandy soils whereas clay helps secure chemicals and roots in the soil.

The *component* table holds the data needed for drainage. The *draingecl* attribute identifies the natural drainage conditions of the soil. Drainage ensures that soil is properly aerated, too much water is capable of choking crops. Soil drainage also reduces soil and nutrient loss from runoff.

The last table used from the SSURGO dataset is the *corestriction* table, this table lists the root restrictive features or layers. The important attribute from this table used in LANDIS-II NECN is the *resdept_r* attribute. *Resdept_r* is the distance from the soil surface to the upper boundary of the restrictive layer. Soil depth has a large impact on soil water-holding capacity within the model (Scheller et al. 2022).

The following table is a key to the fields used:

Table 5 – Table showing the key to creating LANDIS maps from SSURGO data.

| LANDIS Map | SSURG table name | SSURGO column name |
|---|---|---|
| Soil Drain | Component | Drainagecl |
| Wilting Point | Chorizon | Wfifteenbar_r |
| Field capacity | Chorizon | Wthirdbar_r |
| Percent sand | Chorizon | Sandtotal_r |
| Percent clay | Chorizon | Claytotal_r |
| Soil depth | Corestriction | Resdept_r |

**Maps[2]** were various soil organic carbon and nitrogen maps from the West, T.O. (2014) dataset. The initial amount of carbon in the soil maps are divided into *SOM1surfC,* which is carbon in the soil surface, *SOM1soilC is* carbon in the soil sub-

surface, *SOM2C* carbon in the “slow” soil pool, and *SOM3C* carbon held in the “passive” soil pool.

As a fraction of total carbon each carbon pool is (Robbins et al. 2022):

1. SOM1surfC = 0.01
2. SOM1soilC = 0.02
3. SOM2C = 0.59
4. SOM3C = 0.38

From the individual carbon maps an estimation of nitrogen content in the soil is calculated. Each nitrogen map in the use of LANDIS-II is assumed to be a fraction of each carbon map representing the same pools as carbon. The initial amount of nitrogen in the soil maps are divided into *SOM1surfN* which is nitrogen in the soil surface, *SOM1soilN* nitrogen in the soil sub-surface, *SOM2N* nitrogen in the “slow” soil pool, and *SOM3N* nitrogen held in the “passive” LANDIS-II soil pool.

Nitrogen maps were created by multiplying the carbon in that pool by a fraction (described below) while setting a minimum value of 1 to avoid a complete lack of nitrogen.

Each nitrogen map is multiplied by its matching carbon map with the following fractions (Robbins et al. 2022):

1. SOM1surfN = 0.1
2. SOM1soilN = 0.1
3. SOM2N = 0.04
4. SOM3N = 0.118

An example of workflow of this process would be:

$$Total\ carbon\ (West, T.O.2014)\ *\ 0.01\ =\ SOM1surfC$$

$$SOM1surfC\ *\ 0.1\ =\ SOM1surfN$$

**Maps[3]** were obtained from Forest Inventory and Analysis data. After isolating each plot in the study area, the total carbon down dead value at each plot, which is the carbon in tons per acre of woody material 3 inches or greater in diameter on the ground along with their stumps and their roots, was taken and interpolated using inverse distance weighting across the study area providing the dead wood on the surface map. The second map, dead wood of coarse roots, calculated from this value is assumed to be a third of the carbon down dead value following the work of Robbins et al. 2022.

**Maps[4]** representing base flow to streams and storm flow were set to .01 being treated as stationary variables, where they were set without input from outside data sources, in this simulation following the work of other projects using LANDIS-II NECN (Robbins et al. 2022). These maps determine the amount of water runoff and leaching affecting the amount of nitrogen, which then affects the amount of mineral nitrogen in the soil. Stream and storm flow were parametrized further with the help of Robbins (Personal Communication, 03/18/2023) where too low of flow caused NAs in soil temperature calculations.

Dead wood on the surface and dead wood of coarse roots in tons per acre are calculated from Forest Inventory Analysis plots within the area of interest. Taking the carbon down dead (tons per acre) from each plot and running an inverse

distance weighted interpolation to the whole study area. The dead coarse roots are assumed to take a third of that value based on Robbins et al. 2022.

### 4.1.4 Initial Communities

To understand what vegetation species are being simulated within each grid cell, a tree list from Riley et al. 2019 was used. The Riley et al. 2019 tree list is a raster with each pixel value being correlated to tree species and plot data from the Forest Inventory and Analysis (FIA) National Program, which was interpolated across multiple states to create a comprehensive tree list for the US.

From the Riley et al. 2019 tree list, it is possible to understand which species are needed to characterize the study area and what plots the species in the study area come from. Plots from the Forest Inventory and Analysis (Gray et al. 2012) program consist of one field sample site for every 6,000 acres, where field crews collect data on forest type, site attributes, species, and size. Within the raster grid, one can understand what plots are included in the study area as pixel value equates to FIA 'PLOT' IDs. The unique pixel values within the study area were taken into a list and then they are compared to data from Riley et al. 2019 which has information on where each 'PLOT' ID comes from on a state level.

| State_Abbreviation | |
|---|---|
| CA | 19370 |
| AZ | 14132 |
| OR | 4324 |
| NM | 1766 |
| ID | 983 |
| WA | 920 |
| UT | 842 |
| CO | 492 |
| NV | 489 |
| TX | 378 |
| OK | 228 |
| MT | 101 |
| KS | 61 |
| NE | 48 |

Fig. 6 – The amount of unique FIA plots from each state present in the study area.

The FIA data that is needed for this study area comes from the states of California, Arizona, New Mexico, Nevada, Oregon, Washington, Colorado, Iowa, Idaho, Kansas, Montana, Nebraska, Oklahoma, Texas, Utah, and Wyoming. The number of unique plots has a high of 19730 from California to 48 from Nebraska (fig. 6). Through the FIA data from each of these states and the unique plots, the next step is obtaining the unique species present over the study area. LANDIS-II NECN requires each species' age and biomass to form cohorts which is a large analytical task. Each species fell into one of four **model types**, using four different model types was necessary as FIA data was not always complete and did not have the necessary variables for certain species and plots within the study area.

**Model type *a* (eq. 4)** was created through an ordinary least squares (OLS) regression where each species' diameters and heights, provided from FIA data,

were regressed to get the coefficients based on diameter x height relations and age x height relations. Where the coefficients for each species were found from an OLS equation which was then used to inform eq. 4 for each species. Some species did not have the needed FIA data of 'AGEDIA', tree age at diameter, resulting in the need for different allometric equations to estimate tree ages where only biomass and diameter were needed. **Model type *c* (eq. 5)** was applied for all pinyon species using an allometric equation from the work of Gascho et al. 2006 **Model type *e*** (eq. 6), using an allometric equation from Barry 2014 over all California Laurels in the study area. The last model type, **model type *f* (eq. 7)** was used for Curlleaf Mountain-Mahogany applied with an allometric equation Brotherson et al. 1980.

Table 6 – Overview of each FIA SPCD, species name, and model type used.

| FIA SPCD number | Common name | Model Type |
|---|---|---|
| 106, 133, 134, 140, 141, 143 | pinyon species | C |
| 475 | curlleaf mountain-mahogany | F |
| 981 | california laurel | E |
| | All other species | A |

To find each species biomass:

$$biomass = `CARBON\_AG'/0.5 * `TPA\_UNADJ' \quad \text{eq. 1 –}$$

Where biomass is in lbs/acre, 'CARBON_AG' is above ground carbon measured in pounds and 'TPA_UNADJ' is a value that must be multiplied to understand per acre information with both variables from the Forest Inventory and Analysis program. 'TPA_UNADJ' stands for *trees per acre unadjusted,* which represents the number of trees per acre that the sample tree theoretically represents based on the sample design.

As the model needs biomass in grams per meter$^2$ we converted biomass from pounds per acre by:

$$biomass\ g/m2 = biomass\ lbs/acre * 0.112085 \quad \text{eq. 2 -}$$

Converting biomass generated by eq. 1 to g/m$^2$.

Obtaining tree ages is done through fitting an ordinary least squares regression formula as a two-parameter model with interactions. The formula of the ordinary least squares regression:

$$OLS = `AGEDIA \sim DIA * HT' \quad \text{eq. 3–}$$

OLS equation used to obtain coefficients used to inform age (eq. 4).

Where 'AGEDIA' is the tree age at the point of diameter measurement which is either DBH (diameter at breast height) or DRC (diameter at root collar). 'DIA' is the current diameter at time of measurement in inches done either at DBH or DRC. 'HT' is a field that holds the total height of a sample tree in feet from the ground to the top of the main stem. 'AGEDIA', 'DIA', and 'HT' are fields drawn from FIA SITEREE tables.

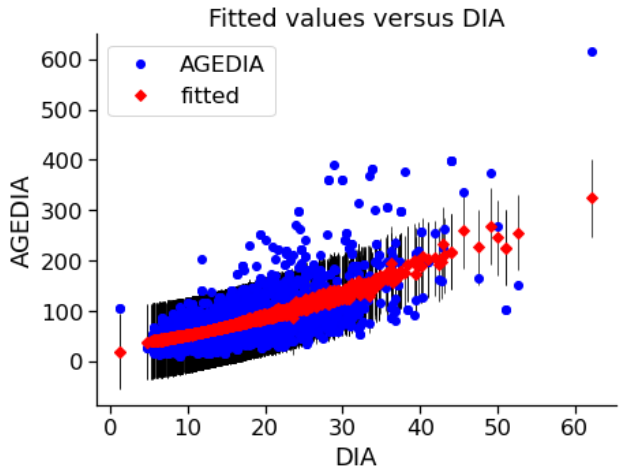


Fig. 7 –AGEDIA x DIA relationship of Jeffrey Pines (SPCD 116) from FIA sitetree tables across the study area. Where AGEDIA is the result of the two-parameter linear regression formula and the fitted being the estimated response.

Then the use of the model form where *ages = aX1 + bX2 + cX1X2 + d* is employed to age species across the study area. This equation is informed by the coefficient results of the ordinary least squares (OLS) and FIA diameter and heights for each species at plot scales and is described as **model type *a*** (eq. 4):

$$ages = OLS\_coefficient.DIA * diameters + OLS\_coefficient.HT * heights + OLS\_coefficient.DIA{:}HT * diameters * heights + OLS\_coefficient.intercept$$ eq. 4 –

Model type *a* ages equation used to determine species age informed by variables acquired from eq. 3.

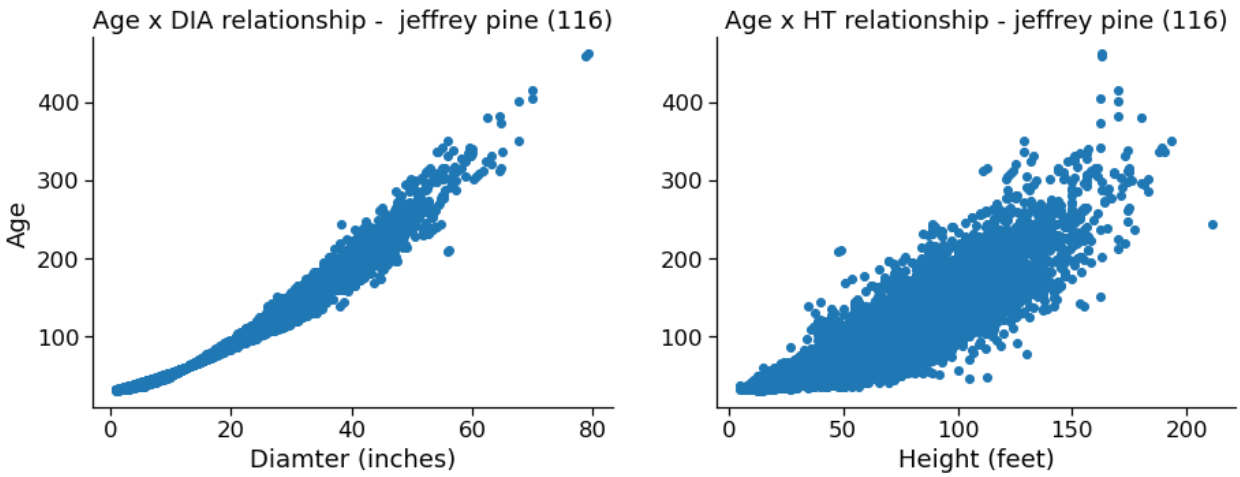


Fig. 8 – Age x Diameter and Age x Height relationship of Jeffrey Pines from FIA tree data across the study area. The Jefferey Pines were aged through eq. 5.

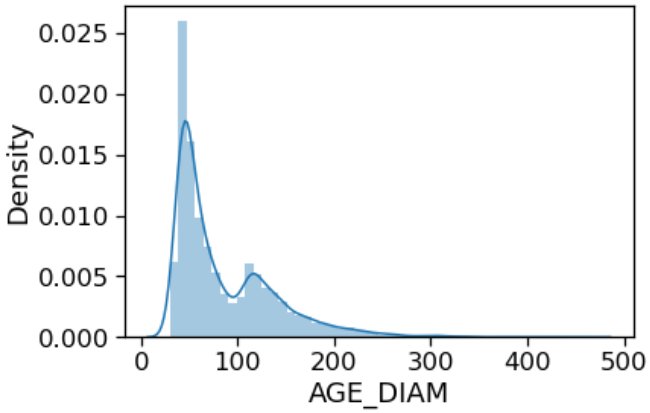

Fig. 9 – AGE_DIAM (Age) distribution plot of Jeffery Pine (SPCD 116).

There are 109 unique species that are modelled under **model type *a*** (eq. 4), with an example of the distributions of age and diameter and age and height relationships being shown in figure 8 and age density distributions being shown in figure 9 for Jeffrey pines across the study area.

There were 6 pinyon species being modelled under **model type *c*** (eq. 5) with an example of singleleaf pinyon relationships being shown in figure 10 and age densities in figure 11.

$$age = (6.69 * x) + 18.5 \; (Gascho\ Landis\ and\ Bailey\ 2006) \qquad \text{eq. 5 –}$$

Age equation for pinyon species where *x* is diameter in centimeters.

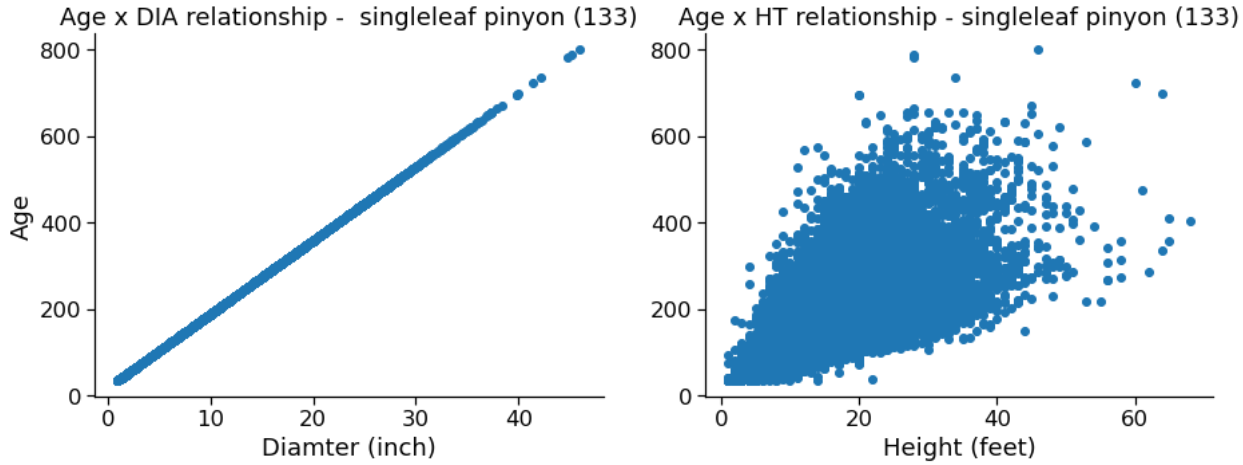


Fig. 10 – Age x Diameter and Age x Height relationship of Singleleaf Pinyons (SPCD 133) from FIA tree data across the study area aged through **model type *c*** (eq. 6).

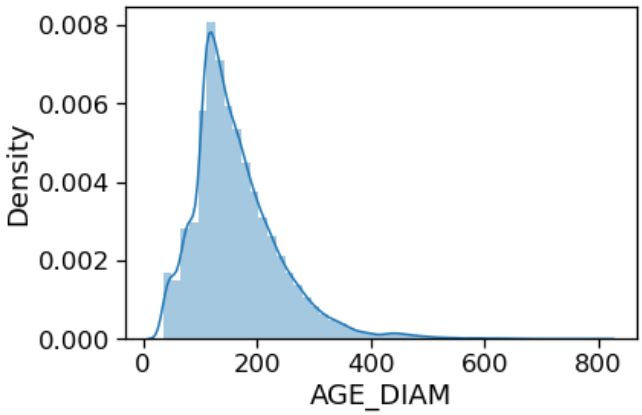


Fig. 11 – AGE_DIAM (Age) distribution of Singleleaf Pinyons (SPCD).

**Model type *e*** (eq. 6) has been used for California Laurel. The age and diameter and age and height distributions for California laurel are shown in figure 12 with a distribution of ages shown in figure 13.

$$age = 1.5519(x) - 29.819\ (Barry\ 2014)$$ eq. 6 –

Model type *e* age equation for California Laurel where x is diameter in centimeters.

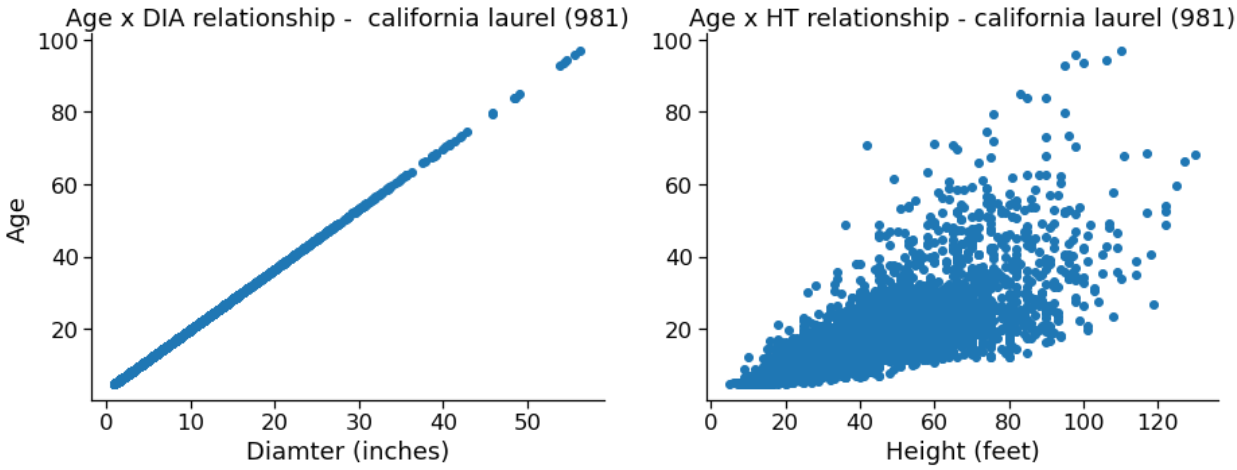


Fig. 12 - Age x Diameter and Age x Height relationship of California Laurel (SPCD 981) from FIA tree data across the study area aged through **model type *e*** (eq. 7).

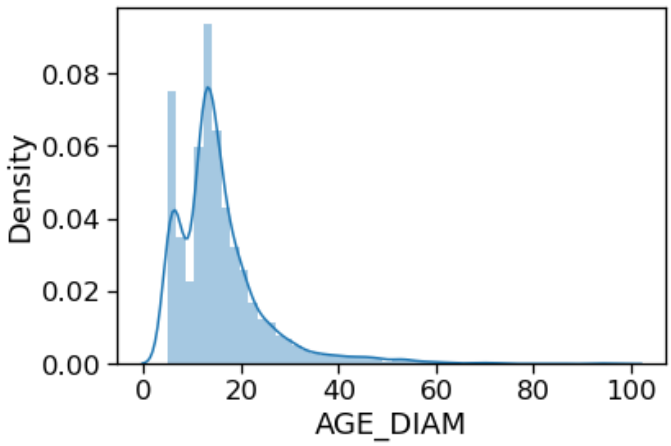


Fig. 13 – AGE_DIAM (Age) distributions of California Laurel (SPCD 981).

The final model type is described as **model type *f*** *(*eq. 7) which was used for Curlleaf Mountain Mahogany. Figure 14 shows the age and diameter and age and height distributions of curlleaf mountain-mahogany with the age distributions across the study area in figure 15.

$$age = (0.4667 * x) + 31.0326\ (Brotherson, Davis, and\ Greenwood\ 1980) \qquad \text{eq. 7 –}$$

Model type *f* age equation for curlleaf mountain-mahogany where x is diameter in millimeters.

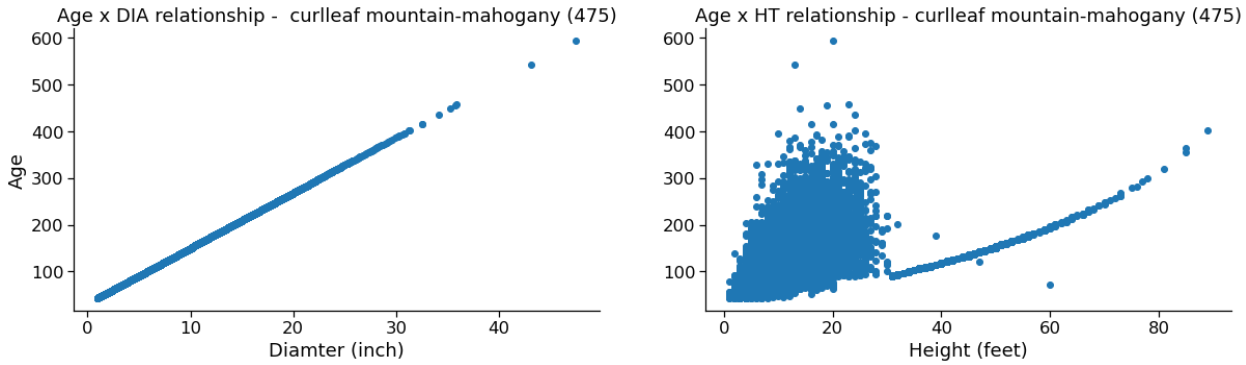

Fig. 14 - Age x Diameter and Age x Height relationship of Curlleaf Mountain-Mahogany (SPCD 475) from FIA tree data across the study area aged through **model type *f*** (eq.8).

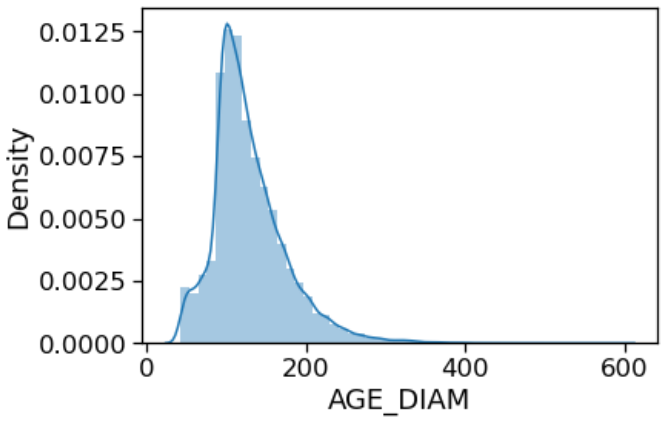


Fig. 15 – AGE_DIAM (Age) distribution of Curlleaf Mountain-Mahogany (SPCD 475).

Age and biomass information was used to create a text file containing the Initial Communities within the study area. This text file is used by LANDIS-II NECN to enable the model to understand every active pixel on the map with each pixel value containing species with biomass and age referenced in the Initial Communities text file. Each active site on the landscape is assigned to an initial community MapCode. The MapCode specifies the tree species that are present along with the age ranges and associated biomass ranges that are present for each of those species at that site.

Data from the Gap Analysis Project (Comer et al. 2003) has been used to fill in non-tree species to include chaparral species, coastal sage scrub, and other grassland species to simulate real world scenarios more with a more accurate fuels continuity.

## 4.2 NECN Model Setup

LANDIS – II reads multiple text files that inform the model of individual species properties, life history, shade tolerance, fire tolerance, initial nitrogen in the soil, and other soil properties evolving over model time steps. Vegetation regeneration was simulated on an annual time step, growth on a monthly time step, and fire on a daily timestep following Robbins et al. 2022. For NECN non-climate CSVs 'NECN_Spp_Table' and 'NECN_Functional_Groups' along with the species properties text file of 'species_props', have been parameterized through following the work of other projects using LANDIS-II NECN (Robbins et al. 2022, Bisquay 2021, Syphard et al. 2011, Liang et al. 2017) and parameterized through the Fire Effects Information System (FEIS) database (Abrahamson 2014) when other projects did not have species specific data in the study area. LANDIS – II also reads in raster maps from table 2 that hold information about initial communities and soil attributes.

## 4.3 SCRPPLE

The disturbance extension of SCRRPLE was published in the summer of 2019, emphasizing climate change and human interactions with the inclusion of different ignition sources, variable fire suppression, and prescribed fires (Scheller et al. 2019). An essential aspect of SCRRPLE is that the cells are spatially interactive, meaning fire spreads across the landscape based on the daily Canadian Fire Weather Index (FWI) (Van Wagner 1974), wind speed, and fine fuels in adjacent

cells (Robbins et al. 2022). Each ignition type in SCRPPLE has its suppression patterns where different levels of fire suppression are determined by the FWI at model time step. SCRPPLE assumes that if suppression is constant, lightning and accidental fires will behave similarly regarding spread and mortality with the same FWI and wind speeds (Scheller et al. 2019).

### 4.3.1 SCRRPLE Parameterization

SCRPPLE is a fire model that is designed to capture. s climate change and landscape-scale changes fire behavior forecasted by climate changeover large study areas (Scheller et al. 2019) through an extensive parameterization process. To parameterize SCRPPLE accidental and lightning ignition, suppression, slope, and uphill slope maps were needed alongside a text file describing ignition coefficients for both lightning and accidental fires, fire spread parameters, mortality parameters, and a suppression input csv. The SCRRPLE text file also has site-level mortality information, probability of daily intercellular spread, and maximum daily spread coefficients and intercepts. Other inputs include maps of lightning and accidental ignition densities and accidental and lightning suppression maps.

Ignition maps are rasters that represent where accidental and lightning ignitions occur. Cells with higher values represent where ignitions are more likely to occur, while values of 0.0 are unable to experience ignitions. Ignitions occur on any day when predicted by a random draw from a Zero-inflated Poisson or Poisson Distribution fitted to observed ignitions (Scheller et al. 2022). From ignition, fire can

spread into adjacent cells, which relies upon a probability of spread out of four nearest neighbors until no more cells are selected to burn. Slope and uphill slope maps are used in the calculation of fire spread. specifying raster maps represent slope as a percent and the direction of uphill slope, The spread calculation uses the coefficients found from a generalized linear model with the dependent variables of effective windspeed and fine fuels derived from LANDFIRE (USGS 2022) data. Fire severity is the mortality caused by fire at each site varying dependent upon tree species and ages present (Scheller et al. 2022), are determined by max bark thickness classes. Suppression rasters represent areas where fires are suppressed with classes of 0 to 3, indicating no suppression, light, moderate, and maximum suppression. That data then relates to the possible suppression scenarios represented within the suppression input csv, which defines the effectiveness of suppression based on each ignition type across different FWI ranges (Scheller et al. 2022).

Table 7 – SCRRPLE parameterization variables needed table.

| SCRPPLE Inputs | Source |
|---|---|
| Fire spread parameters | MTBS fire perimeters 2000-2018 (Nelson 2021). Data was used for preprocessing and validation. Perimeter data was used to help parameterize spread probabilities as well. |
| Fire Weather Index (FWI), Daily | Daily FWI is calculated according to the LANDIS Climate Library (Lucash et al. 2017). Validation FWI climate data has been provided from gridMET (Abatzoglou 2013) downloaded by Zachary Robbins. |
| Fuel Map | Fuel map used to calculate spread parameters based on LANDFIRE 2020 Existing Vegetation Cover (USGS 2022) |
| Daily wind direction | Calculated from historical climate data windspeed, slope, and uphill slope azimuth to inform parameterization of fire spread |
| Ignition Coefficients | Short 2021 fire ignition data used in relation to FWI to fit a zero inflated possion model where the coefficients inform a scrpple text file |
| Elevation, Slope, and Uphill Slope Azimuth maps | 2020. 1 Arc-second Digital Elevation Models (DEMs) - USGS National Map 3DEP Downloadable Data Collection |

| | |
|---|---|
| | *Geospatial_Data_Presentation_Form:* raster digital data |
| Accidental and Lightning Ignition Maps | Short 2021 fire ignition data used to create density maps of accidental and lightning ignitions |
| Accidental and Lightning Suppression Maps | Created from current urban areas (Radeloff et al. 2018), TIGER/Line 2019 shapefile from the US Census Bureau, and wilderness areas from the University of Montana (wilderness.net) |
| Species bark thickness | Species bark thickness was found through FIA data and bark thickness equations described below. Was used to parameterize cohort level mortality. |
| Suppression Input CSV | Used to assign suppression effort based on FWI and mapcodes from Accidental and Lightning Suppression maps. |

Using SCRPPLE analyzing fire frequency and intensity within the wildland-urban interface zones for 2050 and 2100 within my study area was possible. The first step in the parametrization of this model was preparing a digital elevation model (DEM) at 100m so the model would be informed of elevation, slope, and uphill slope. Elevation in meters was the direct product of a DEM (USGS 2022), whereas slope was found using QGIS (QGIS 2023), and that product was then used in R (R Core Team 2022) to compute aspect and then convert to uphill slope aspect.

The next step in parameterization was to find model ignition coefficients. Within SCRPPLE where ignition can occur on any day, the numbers of fires are given as a random draw from a Poisson Distribution (Scheller et al. 2022). Ignition coefficients are used in the fitting of a four-parameter model by ignition type used within SCRRPLE (Scheller et al. 2022). Ignition coefficients were found following the work of Robbins et al. 2022 parametrized using Short 2021 ignition database, LANDIS-II climate library (Lucash et al. 2017) and gridMET historical weather data (Abatzoglou 2013), where a zero-inflated Poisson model of the likelihood of each ignition type is fit to the daily fire weather index. Ignition data is taken and

segregated into accidental and lightning ignitions. Then, each ignition type data is merged based on a unique date id to historical climate data with the included FWI.

Table 8 – Results of zero inflated model lightning and accidental ignitions.

| **Ignition Type** | **Count Model B0** (Poisson with log link) | **Count Model B1** (Poisson with log link) | **Count Model B0 Pr(>\|z\|)** (Poisson with log link) | **Count Model B1 Pr(>\|z\|)** Poisson with log link) | **Zero-inflation Model B0** (Binomial with logit link) | **Zero-inflation Model B1** (Binomial with logit link) | **Zero-inflation Model B0 Pr(>\|z\|)** (Binomial with logit link) | **Zero-inflation Model B1 Pr(>\|z\|)** (Binomial with logit link) |
|---|---|---|---|---|---|---|---|---|
| Accidental | -1.855520 | 0.049388 | 2.23e-14 | 6.14e-11 | 3.15083 | -0.09067 | < 2e-16 | 1.36e-12 |
| Lightning | -5.79616 | 0.16850 | 9.65e-07 | 6.43e-07 | 2.63789 | 0.02036 | 0.0159 | 0.5040 |

Table 8 shows the results of the zero inflated model with count model family of Poisson. The results of the models suggest that within the lightning ignition model the coefficients from the count portion and intercept from the zero-inflation portion coefficients are statistically significant. While the results from the accidental ignition model suggest that the predictors in both count and the inflation portions are statistically significant. It was important to use zero-inflated Poisson for the data because between the historical climate data and ignition data there are lots of days that did not experience ignitions making the fit of models to the data poor when using non-zero-inflated models. The coefficients of both the count model and zero-inflation model were then used to inform SCRPPLE of lightning and accidental ignition $B_0$ and $B_1$.

Using the zero-inflated Poisson models it was possible to simulate lightning and accidental ignitions within the time frame of the observed data.

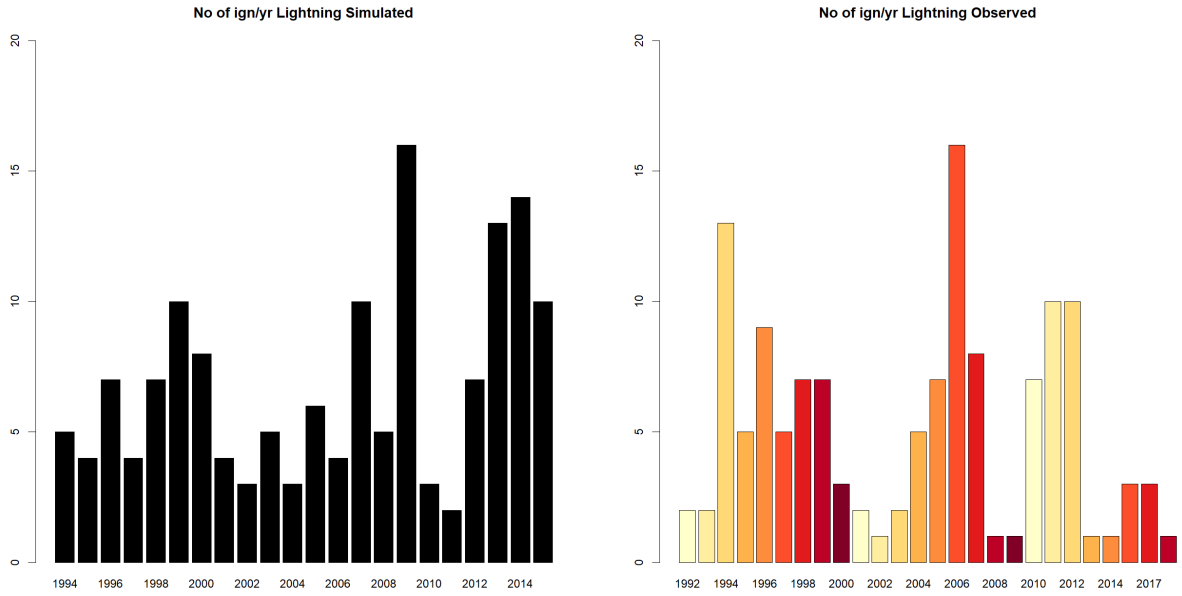


Fig. 16 – Zero-inflated Poisson lightning simulations compared to lightning observed.

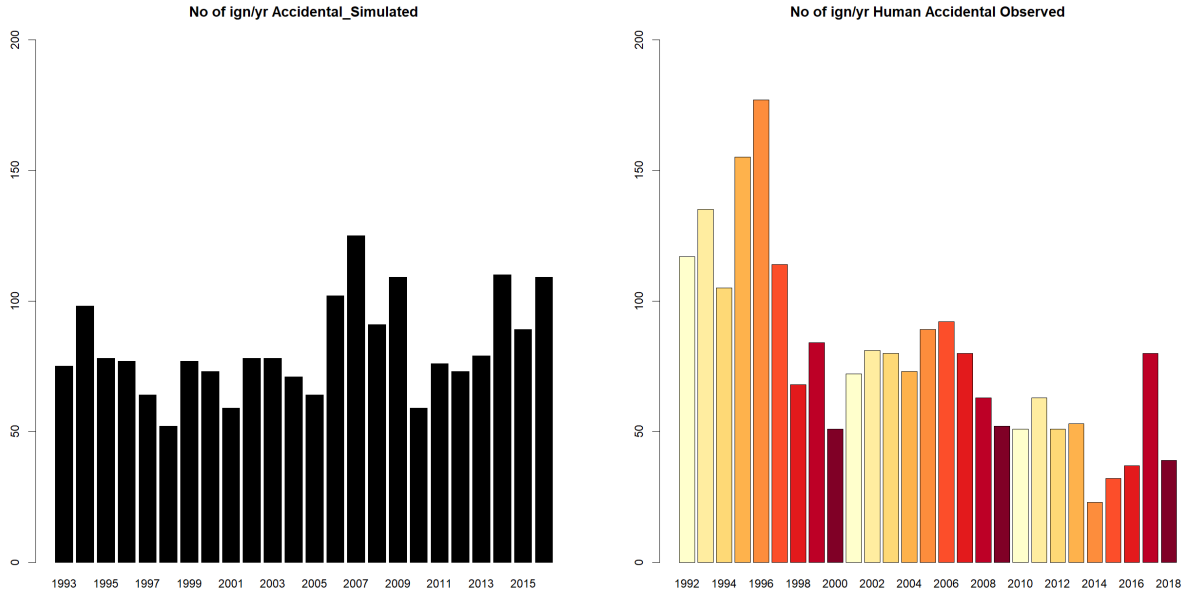


Fig. 17 – Zero-inflated Poisson accidental simulations compared to accidental observed.

Over the same year period as observed (1992-2018), the simulated values with zero-inflated Poisson model (R, R Core Team 2022) informing the simulation found 1781 accidental ignitions against the observed period which saw against the

observed period which saw 1939 accidental ignitions with the simulated difference of 8.2% simulated lightning ignitions 37 lightning ignitions compared to 122 observed which was a +12.3% difference compared to that observed period suggesting that the coefficients used were also ready to be input into the SCRPPLE text file completing the ignition coefficients. It is important to note that these R simulations were stochastic.

Fire spread parameters were found by following Robbins (2021). Spread parameters are informed by LANDFIRE 2020 (USGS 2022) existing vegetation cover fuels data for the study area, uphill slope azimuth in degrees, and slope as a percentage where uphill slope and slope are used to calculate the direction of fire spread. Historical climate data was combined to date and ecoregions as a data frame. A raster stack was created, complied of a wind map, fuel map, uphill slope, and slope. Then the historical fires shapefiles are filtered to only include shapes that are not just the final burn shape for fire spread to be calculated. Once the shapes fires were filtered again on the criteria having more than one day of spread to select the fire perimeter from the first day and then select the second to calculate the area of expansion to find fire spread on a cellular level. The climate and fuel variables from the climate stack were extracted to compile a data frame of every cell within the fire perimeters (Robbins et al. 2022).

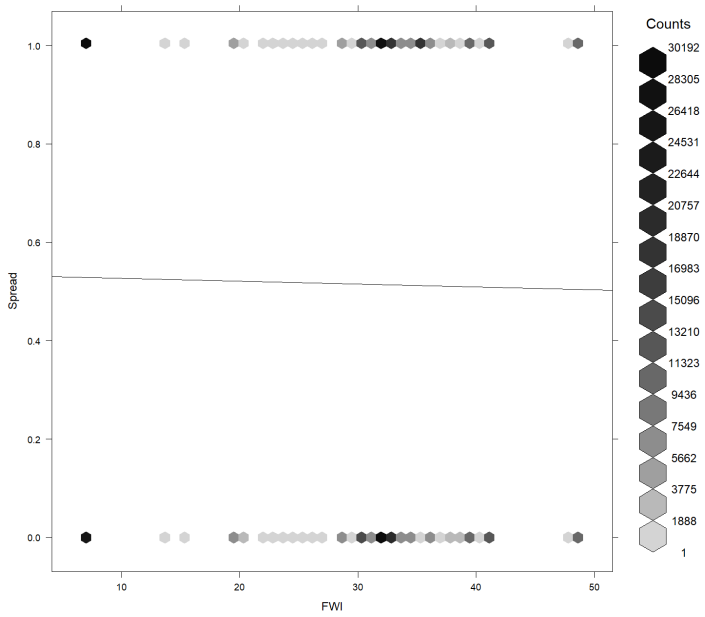


Fig. 18 – Relationship between FWI and cellular probability fire spread.

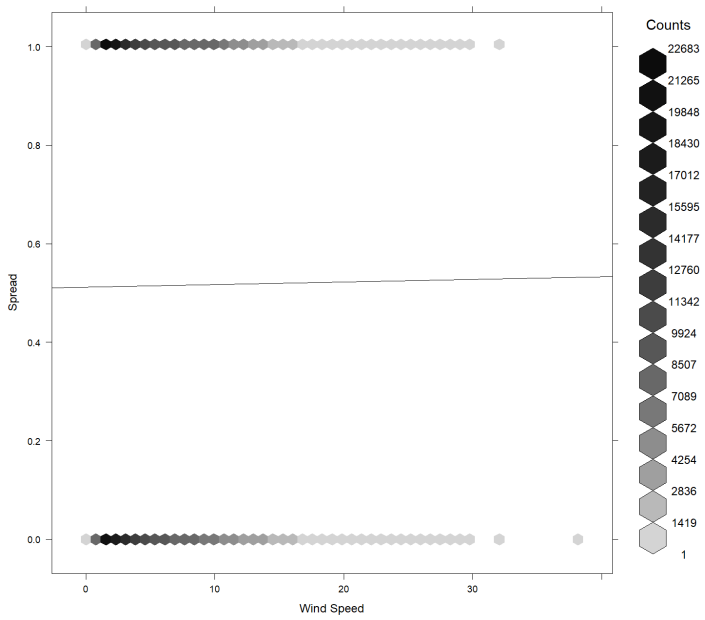


Fig. 19 – Relationship between wind speed and cellular probability fire spread.

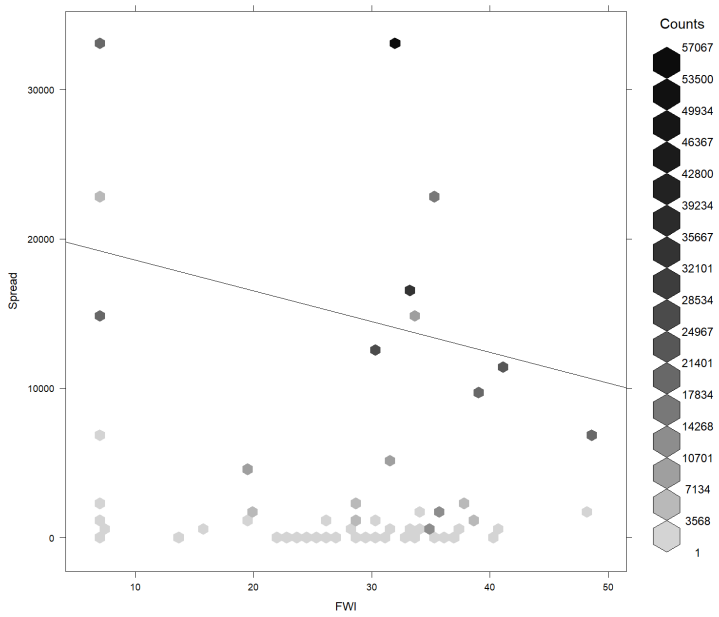


Fig. 20 – Relationship between FWI and spread total cellular expansion.

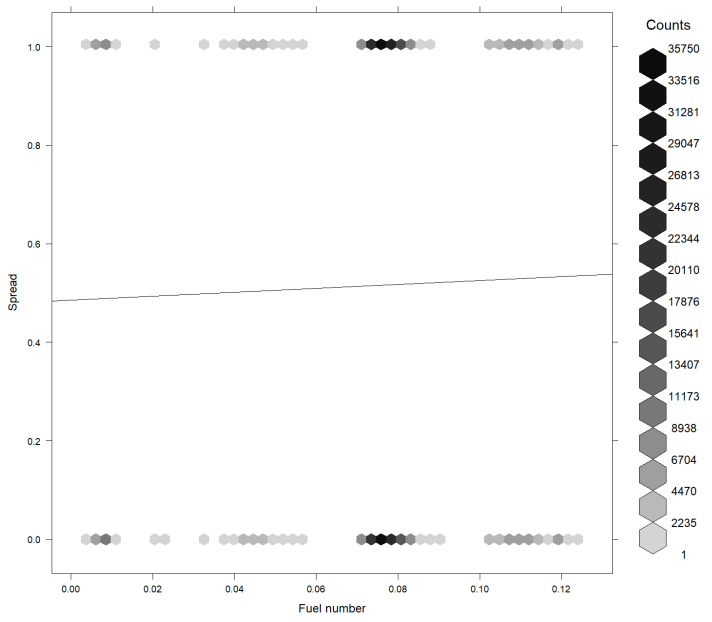


Fig. 21 - Relationship between wind speed and spread total cellular expansion.

Spread in the area of interest is characterized by wind speed having more impact on fire spread rather than FWI (Fig 18-21). The stronger relationship can be easily seen in fig. 22 and 23 when looking at total cellular expansion of historical

fires. In the model SCRPPLE text file, since FWI did not impact cellular spread a generalized linear model (glm) with the dependent variables of effective windspeed and landscape fuels was used to obtain spread coefficients for intercellular fire spread.

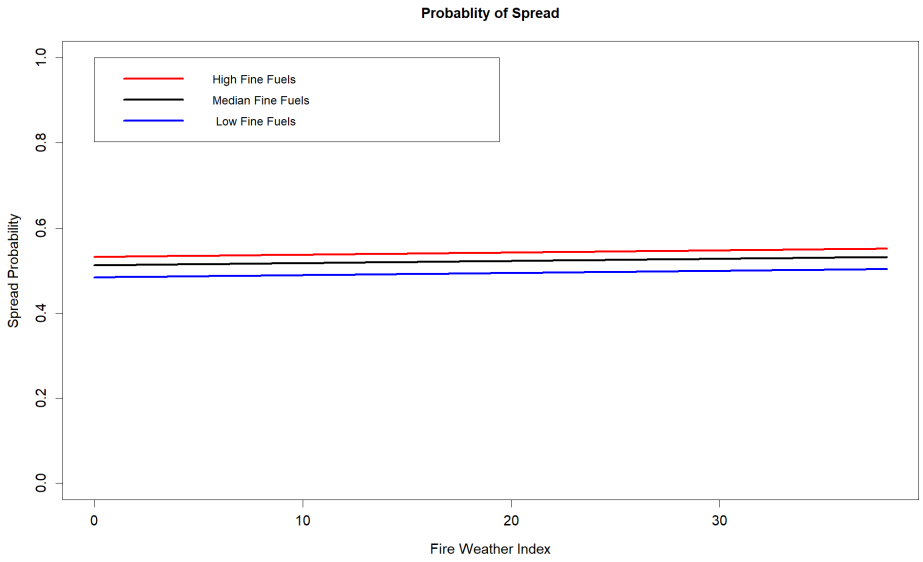


Fig. 22 – Intercellular spread probability based off glm spread coefficients for different fine fuel classes.

The results of a glm formed the SCRPPLE text file intercellular spread coefficients of $B_0$ $(-0.0719755)$, $B_1$ (1.6034705), and $B_2$ $(0.0020485)$. The coefficients from the glm formed the basis of fig. 22 showing the spread of different fuel classes. The last parameter of fire spread for SCRPPLE was maximum daily spread coefficients, which were found through a linear model using the historical climate FWI and windspeed data over the area of interest as the dependent variables providing the coefficients of $B_0$ $(-2224.19)$, $B_1$ (82.06), and $B_2$ $(364.25)$.

Once coefficients were found for daily intercellular spread probability, maximum daily spread, and accidental and lightning ignitions, finding bark thickness per species was needed to inform site-level mortality coefficients in the SCRRPLE text file. Specific bark thickness was calculated from a set of equations found in different bodies of literature (Rebain et al. 2022, Kozak and Yang 1981, Zeibig-Kichas et al. 2016, McDonald 1983, Schafer et al. 2015) to produce bark thickness in inches of the oldest species of each species type across the study area. Specific bark thickness of each species was then used to inform a mortality model (Robbins et al. 2022) where each species would be binned into 5 bark thickness classes to allow species to respond to fire severity and mortality based on bark thickness. Unlike Robbins et al., 2022, field-based data to calculate likelihood of mortality was not available. Instead, fire tolerance ratings based on bark thickness and expert understanding of fire tolerance was used.

The first equation was from The Fire and Fuels Extension to the Forest Vegetation Simulator (FEE-FVS) using FEE-FVS coefficients (Rebain et al. 2022) based on tree species within the study area. With the equation of (eq. 8):

$$Bark\ Thickness\ =\ Vsp(D) \qquad \text{eq. 8 –}$$

Where Vsp is the species multiplier provided by FEE-FVS and D is species diameter in inches provided from FIA data.

Four other equations were used to identify species bark thickness when FEE-FVS did not have species specific data.

$$Bark\ Thickness\ =\ D/2\ (1-k) \qquad \text{(Kozak and Yang 1981)} \qquad \text{eq. 9 –}$$

Where *d* is diameter at breast height outside bark (DHOB), and *k* the regression coefficient for the relationship of diameter inside bark (DIB, d) to DOB.

$\sqrt{BarkThickness} = a * \sqrt{DBH}$ (Zeibig-Kichas et al. 2016) eq. 10 –

Where *a* and b are a species related coefficient and DBH is diameter at breast height.

$Bark\ Thickness = -1.693 + 0.0219x + 1.2813x^{-1}$ (McDonald 1983) eq. 11 –

Where Vsp is the species multiplier provided by FEE-FVS and D is species diameter in inches provided from FIA data.

$Bark\ Thickness\ (mm) = \ 0.835 * x^{0.797}$ (Schafer et al. 2015) eq. 12 –

Where x is DIA in centimeters.

. Maximum *bark thickness* for the species in the study area was then binned into classes based on an R script (Robbins, personal communications, 03/01/2023). This process assigned a *bark thickness* variable between 3, 2.5, 2, 1.5, and 1 to each species depending on the max *bark thickness* provided from the equations (eq. 8, 9, 10, 11, 12) used. With a range of 20 – 10cm assigned to class 3, 9 – 7cm assigned to class 2.5, 6 - 5cm the class 2, 4 – 2cm the class 1.5, and 1 – 0.1 cm a class of 1. These classes create a simple SCRPPLE mortality assuming a relationship between ladder fuel (0-1000 g/m2) and fine fuel (0-1, scaled by max fuel) and effective windspeed working as a heuristic understanding of mortality.

Table 9 – Showing each species and what equation calculated bark thickness.

| FIA SPCD number | Common name | Bark Thickness Equation |
|---|---|---|
| | All other species | Eq. 8 FEE-FVS (Rebain et al. 2022) |
| 93, 96, 242, 263, 264, 312, 313, 321, 322, 351, 352, 353, 375, 745, 747, 748, 749 | Assorted spruces, hemlocks, maples, alders, paper birch, and cottonwoods | Eq. 9 (Kozak and Yang 1981) |
| 81, 201, 202 | Incense cedar, bigcone douglas-fir, douglas-fir | Eq. 10 (Zeibig-Kichas et al. 2016) |

| | | |
|---|---|---|
| 361, 362 | Pacific and Arizona madrone | Eq. 11 (McDonald 1983) |
| 823, 826, 827, 829, 834, 835, 838, 843, 846, 847 | Assorted oak species | Eq. 12 (Schafer et al. 2015) |

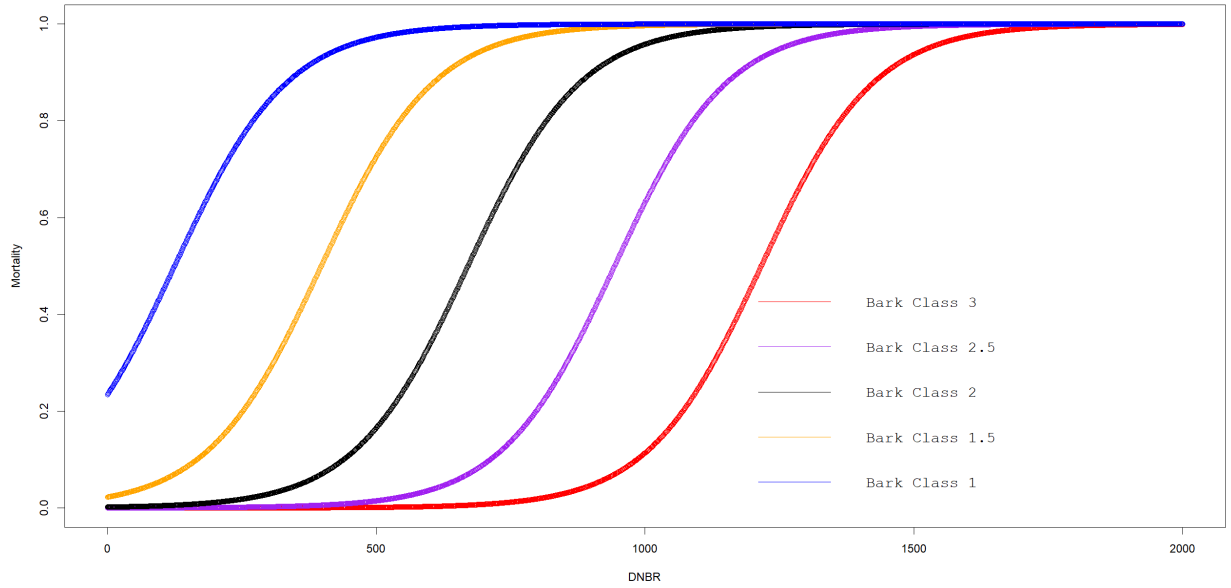


Fig. 23 – Plot showing how different bark classes respond to levels of DNBR/severity and mortality.

Fig. 23 shows how the different classes of bark thickness respond to varying levels of DNBR/burn severity of fire. The y-axis shows mortality of species in each category. This relationship assumes that all species put on bark due to age in the mortality curves. From these relationships cohort level mortality was found from a linear model provided from Robbins et al. 2022 of $B_0$ of .01, $B_1$ of -7 fit to the relationship between bark thickness and cohort mortality and $\text{and } B_2$ of 0.0095 fit to the relationship between site mortality and cohort mortality. Cohort mortality coefficients were provided from Robbins (personal communication, 2023).

Ignition maps were created from accidental human ignitions and lightning ignitions which were interpolated from the fire record of 1992-2018 (Short 2021).

Ignition maps for SCRPPLE were created based on historical accidental and lightning ignitions, where each pixel is assigned, a density based on a probability spatial distribution map in the area under each ignition type. Ignitions are distributed spatially using a probability distribution map for each ignition type.

To parameterize wildfire suppression, historical burned area between 2000-2018 for each suppression type was matched within +/-10% from LANDIS simulated burned area. SCRPPLE allows variable suppression effort and effectiveness dependent on FWI (Robbins et al. 2022) through a suppression input csv. The suppression input CSV defines suppression effort when fire is met at a range of FWI, to get close to historical recorded burn areas suppression efforts were altered over numerous simulations. I defined suppression levels using a combination of wildland-urban interface maps (Radeloff et al. 2018), maps of roads, topography using ridgelines, and wilderness-designated areas provided by the University of Montana Wilderness Institute following the work of Deak 2022.

Table 10 – Suppression input table.

| IgnitionType | Mapcode | Suppress_Category_0 | FWI_Break_1 | Suppress_Category_1 | FWI_Break_2 | Suppress_Category_2 |
|---|---|---|---|---|---|---|
| Accidental | 0 | 0 | 13 | 0 | 25 | 0 |
| Accidental | 1 | 20 | 13 | 40 | 25 | 60 |
| Accidental | 2 | 35 | 13 | 50 | 25 | 70 |
| Accidental | 3 | 50 | 13 | 70 | 25 | 80 |
| Lightning | 0 | 0 | 13 | 0 | 25 | 0 |
| Lightning | 1 | 0 | 13 | 0 | 25 | 25 |
| Lightning | 2 | 10 | 13 | 10 | 25 | 50 |
| Lightning | 3 | 40 | 13 | 40 | 25 | 80 |

The suppression input table defines suppression effort based on FWI and Mapcode. Mapcode is defined from accidental and lightning ignition suppression

maps. Mapcode 3 was the wilderness-designed areas, Mapcode 2 was current urban areas, and Mapcode 1 was study area ridgelines (Deak 2022). The value *"Suppress_Category_0"* indicates the suppression effort, out of 100, when FWI is below "*FWI_Break_1",* when FWI is equal or above 13 suppression efforts are kicked up to *"Suppress_Category_1",* when FWI is then above "*FWI_Break_2"* *"Suppress_Category_2"* activates where the suppression effort defines how much the probability of spread is reduced by suppression efforts (Scheller et al. 2022).

## 4.4 WUI Creation

Our model aims to simulate how fire may interact with urban growth/WUI boundaries. Urban growth projections (Sohl et al. 2014) was be used to view the study area's urban growth to the year 2100. The wildland-urban interface is an area where houses and people mix with undeveloped wildland vegetation (Radeloff et al. 2005). No WUI projections exist for the year 2050 or 2100. To create a "WUI" from projected urban growth, a buffer of 1.5mi on both sides of the urban growth polygon will be applied, following roughly Radeloff et al. 2005 assessment of the WUI. This "WUI" is an idea of what could be as development projections are not coupled into LANDIS-II or SCRPPLE. Planned urban growth will only impact vegetative growth, which the lack of accounting for in the modeling process presents a weakness in this work.

The US government has defined the wildland-urban interface definition in the *Federal Register* (USDA 2011) and has been used in the past WUI assessments

(Radeloff et al. 2018, Radeloff et al. 2005). WUI has been separated into interface and intermix, the intermix where houses and wildland vegetation merge and interface where human areas have <50% vegetation but are within 1.5 miles of densely vegetated areas (Radeloff et al. 2018). WUI being both intermix and interface, for the sake of LANDIS-II WUI-Fire analysis, I have defined the WUI as an urban area which lies within 1.5 miles of densely vegetated areas. To understand densely vegetated areas, I have used the initial communities map that LANDIS-II NECN is running on.

The WUI is 1.5 miles buffered from US census developed areas using 2019 TIGER/Line Shapefiles merged to the California Department of Forestry and Fire Protection Incorporated Cities shapefile to form a comprehensive urban area. Projected urban areas resulted from the work of Sohl et al. 2014 which modeled landcover change predictions for the conterminous United States to the year 2100. I am using the A1B population growth scenario, which was applied for WUI-Fire exchange analysis for the years 2050 and 2100. A1B assumes a population increase of 8.7 billion by 2050 and declining to 7 billion by 2100. A1B suggests that there will also be higher energy demands and is deemed to be more economically focused than other scenarios (Sohl et al. 2014). The increased energy demands and more economically focused population growth scenario better-fit climate scenarios for RCP 8.5, which is suggested to continue to be the best match out to the midcentury under current policies with highly plausible levels of CO2 emissions to

2100 (Schwalm, Glendon, and Duffy 2020).

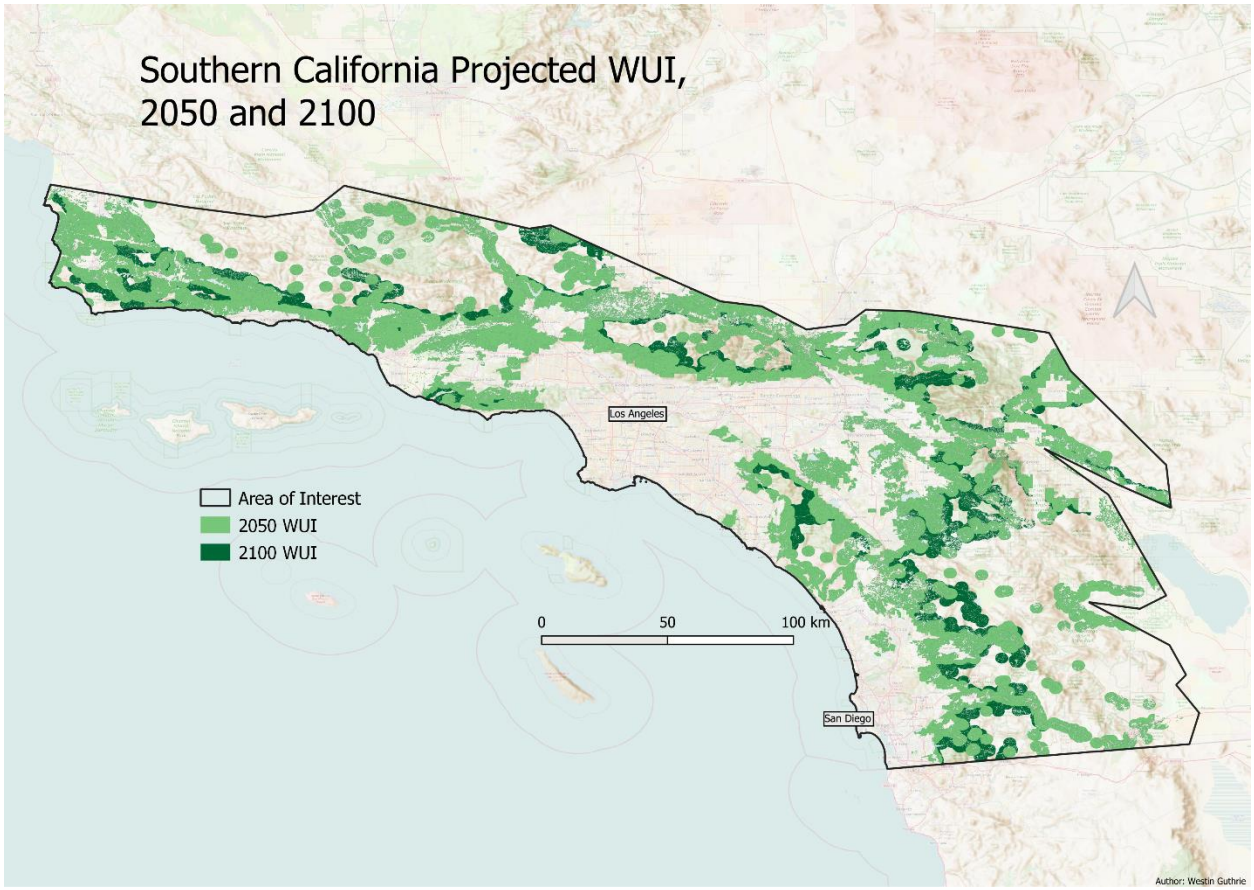


Fig. 24 – Map showing where projected 2050 and 2100 wildland urban interface/intermix areas. The 2100 area includes 2050 plus additional projected expansions.

## 5.0 Model Validation

Each species was run for ten years following an FIA plot species to validate biomass and forest growth. Species validation was done over ten years as FIA plots have a return interval ~ 10 years if a return was done at all. Below are the results from this validation method over the top 5 species: Ponderosa Pine (SPCD 122), Douglas-Fir (SPCD 202), White Fir (SPCD 15), Jeffrey Pine (SPCD 116), and Canyon Live Oak (SPCD 805) in terms of biomass over the study area. FIA returns

to some plots and some species every ten years; using the unique identifiers to identify the recurring species of a plot, I match the growth rate of FIA species to an NECN-simulated species over a ten-year period to match FIA returns. Species not in a plot return interval were matched to a species in the species group or genus.

Table 11 – Results from validation of the top 5 biomass species.

| PLOT_ID (CA) | Name | Initial FIA Biomass (g m/2) | Ten Year Return FIA Biomass (g m/2) | Modeled Biomass (g m/2) | Modeled Percent Difference |
|---|---|---|---|---|---|
| 97120 | Jeffrey Pine (SPCD 116) | 789 | 1356 | 1384 | 2.07% |
| 84235 | Jeffrey Pine (SPCD 116) | 417 | 642 | 648 | 0.93% |
| 87591 | Ponderosa Pine (122) | 897 | 1487 | 1501 | 0.94% |
| 95333 | Ponderosa Pine (122) | 1116 | 1722 | 1606 | -7.20% |
| 66134 | White Fir (SPCD 15) | 527 | 747 | 747 | 0% |
| 62852 | White Fir (SPCD 15) | 378 | 468 | 499 | 6.62% |
| 63757 | Canyon Live Oak (SPCD 805) | 432 | 603 | 548 | 10.04% |
| 81534 | Douglas-Fir (SPCD 202) | 629 | 1478 | 1480 | 0.52% |

The goal was to have the simulated growth be within +/- 10% of recorded growth from FIA of a specific plot tree. Only one species', Canyon Live Oak, simulated growth was over 10% recorded at +10.04%. This variation may account for not every tree experiencing the same growth rate. Different sites can result in a disparity between topographic conditions and different solar and water resource distributions, consequently influencing tree growth (Ma et al. 2018). Elevation and

stand density can also impact species growth (Yeh and Wensel 2000). Due to the interpolated tree map used for initial communities, the site conditions present in the real world for plot 95333 and where plot 95333 is on our interpolated tree map may not be the same.

Once all the species in the study area were properly matched to an FIA plot species, I ran each species for 100 years, reviewing how they grew and ensuring they did not die before reaching their natural longevity. Ensuring “natural” growth was achieved required examining the life history parameters of longevity per species to validate they did not randomly encounter mortality or unlikely loss of biomass outside of disturbance and longevity (Robbins et al. 2022, Bisquay 2021, Syphard et al. 2011, Liang et al. 2017, Abrahamson 2014).

SCRPPLE has been validated by assessing model accuracy by model outputs of accidental human-ignited fires will be compared to observed fires from 2000 -2018 (Short 2021), with the exact comparisons being made for lightning-ignited fires. The mean total area burned in simulations and from historical record of 2000 -2018 will then be compared to hectares burned observed by GeoMAC fire perimeters (Walter et al. 2011).

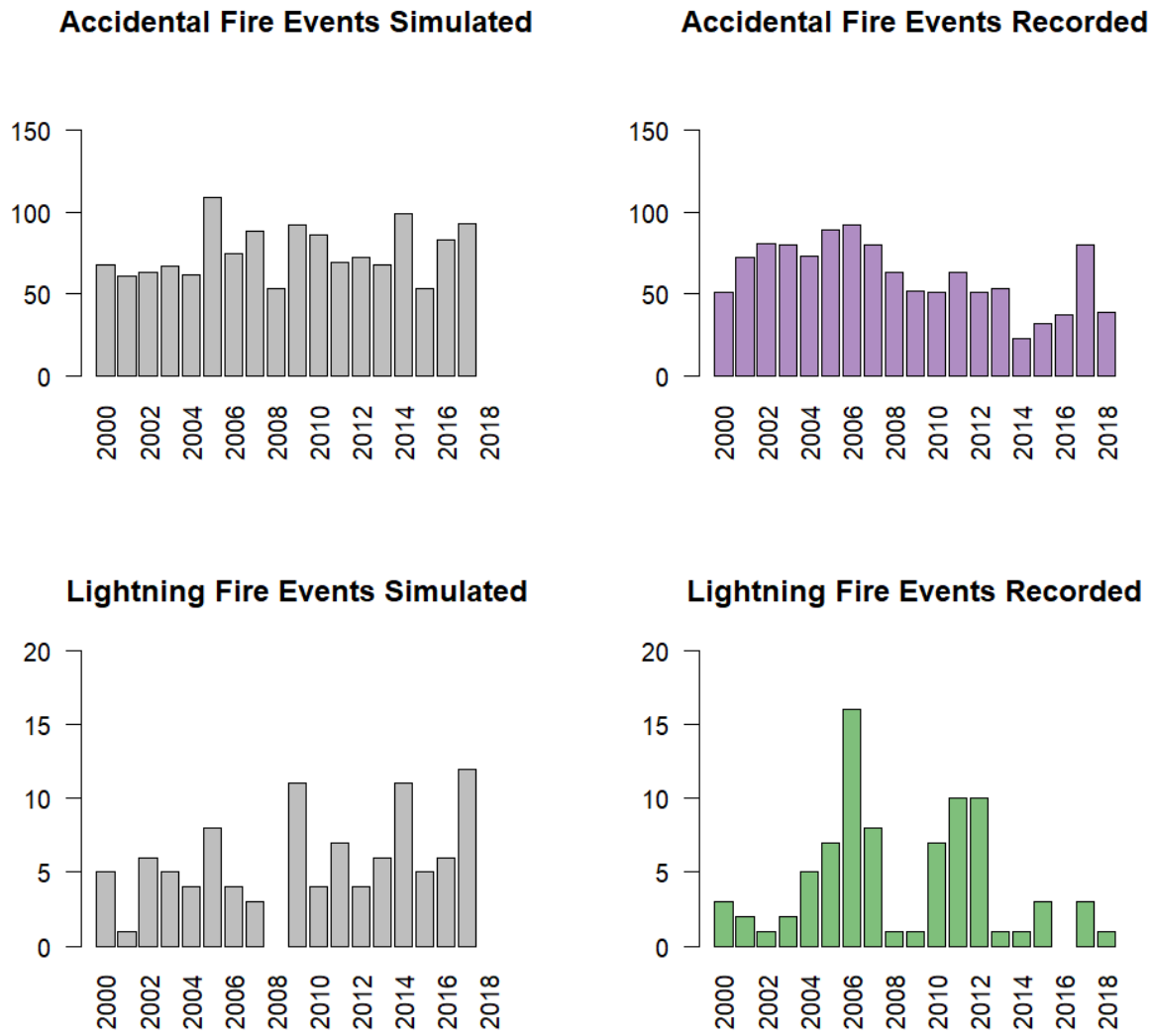


Fig. 25 – Accidental and Lightning ignitions simulated vs observed from Short 2021 and Walters et al. 2011.

Table 12 – Showing the results of validation run accidental and lightning ignitions compared to observed.

| Ignition Type | Simulated Ignitions Amounts over 18-yrs | Observed Ignition Amounts over 18-yrs | Percentage Difference (Simulation vs Observed) |
|---|---|---|---|
| Accidental | 1367 | 1157 | +15.38% |
| Lightning | 98 | 81 | +19.51% |

Within the validation period (2000 – 2018), the study area experienced 1238 total fires. Under the validation run, the study area experienced +18.34% simulated ignitions compared against historical conditions. When compared to Robbins (personal communication, 2023) validation which saw a underestimation of accidental ignitions of -14.34% and an overestimation of lightning ignitions of 8.57% where my work has overestimated both accidental and lightning the accidental simulated results are within a similar range of difference. The burned area increased under the simulated validation run at 3,193,662 ha burned. Over the 2000-2018 period GeoMAC burn perimeters (Walter et al. 2011), and fire ignition data (Short 2021) show that the study area experienced 2,953,058 total ha burned with the simulation predicting a +7.83% higher burned area over 18-year period. Robbins et al. 2022 saw a range of variation between -7.6% to +3.8% across multiple runs suggesting that the simulated validation values aren't far outside of other work.

## 6.0 Results

Table 13 – Climate scenario/model and the global climate model associated with it.

| Climate Scenario/Model | Climate Data Used |
|---|---|
| Greater Precipitation | cnrm_cm5_rcp85 |
| Mean Precipitation | gfdl_esm2g_rcp85 |
| Less Precipitation | miroc-esm-chem_rcp85 |

My research question sought to answer how different climate models impact WUI fire severity and frequency and in the two landmark years of analysis, 2050 and 2100, and in all three climate scenarios, the wildland-urban interface was heavily

impacted by fire. Within all three 2050 scenarios, the WUI saw 1,194,328 ha burned out of 1,279,946 ha of WUI-classified land, which is 93.3% of the WUI experiencing fire in 2050 alone. Out of the three climate scenarios, *Greater Precipitation* experienced the highest number of ignitions in 2050 within and out of the WUI, with over half of 2050 ignitions (50.5%) originating from WUI-classified areas. *Mean Precipitation* resulted in 59% of ignitions in the WUI in 2050, the highest percentage of WUI ignition amongst the models assessed. The final climate scenario of *Less Precipitation* experienced the least number of ignitions within the WUI at 42.6%.

Table 14 – 2050 and 2100 total ignitions and WUI ignitions.

| Climate Scenario | 2050 WUI Ignitions | 2050 Total Ignitions | 2100 WUI Ignitions | 2100 Total Ignitions |
|---|---|---|---|---|
| *Greater Precipitation* | 48 | 95 | 55 | 89 |
| *Mean Precipitation* | 39 | 66 | 38 | 75 |
| *Less Precipitation* | 32 | 75 | 52 | 103 |

2100 saw the total WUI area increase in size to 1,568,840 ha across the study area. Similar to 2050, the 2100 area burned was very similar across scenarios. *Greater* and *Less Precipitation* saw the same amount of WUI land burned at 1,469,365 ha at 93.6% of the WUI, with only the *Mean* scenario experiencing more burned WUI area at 1,470,234 ha, which was 93.7% of the WUI area during 2100. *Greater Precipitation* saw 61.7% of ignitions in the WUI, with *Mean* at 50.6%, and finally *Less Precipitation* at 50.4%.

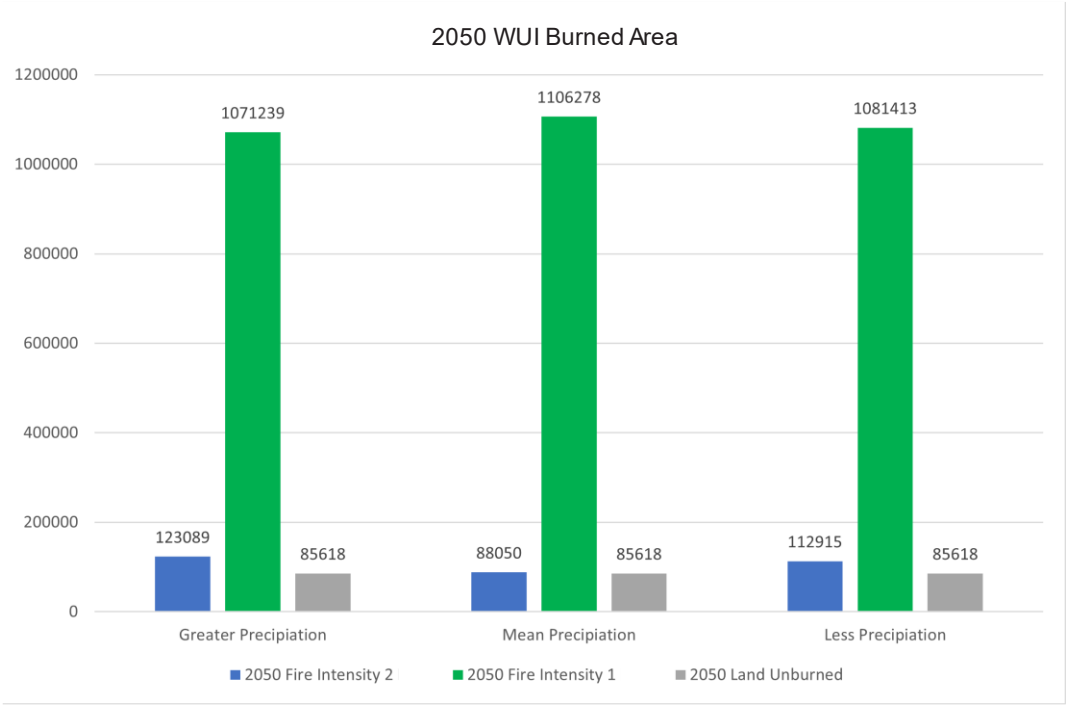


Fig. 26 –WUI land burned within 2050 across all climate scenarios.

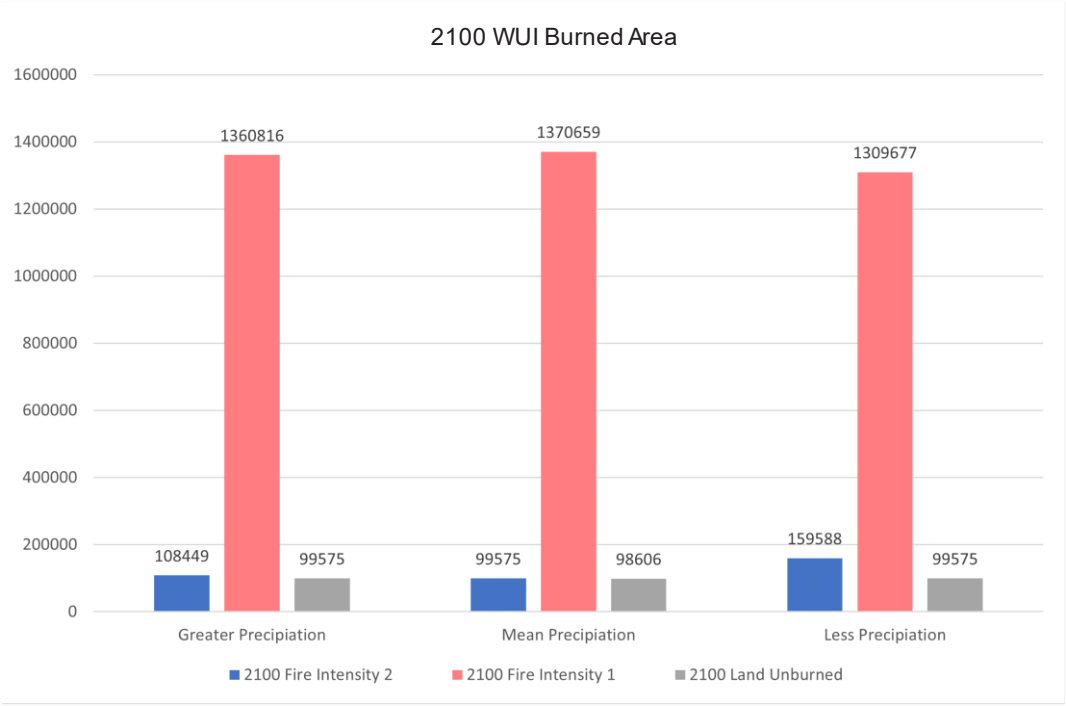


Fig. 27 –WUI land burned within 2100 across all climate scenarios.

## 6.1 Discussion

The results from the three climate scenarios regarding NEEC and AGNPP show the study area was becoming less productive. Across all three scenarios NEEC starts $\sim -80\ g\ c\ m/2 - 1$ indicating that the environment is taking in 80 g c m/2 -1 of atmospheric carbon dioxide. With each climate scenario simulation, it is possible to see that NEEC productivity across the landscape was reduced with carbon taken from the atmosphere ending around $\sim -30\ g\ c\ m/2 - 1$. The reduction in NEEC productivity can also been seen reflected through AGNPP where aboveground net primary production is a measure of plant carbon and energy capture estimated by annual biomass accumulation. NEEC can be understood as the gross primary production of carbon minus ecosystem respiration (Lovett, Cole, and Pace 2006) where ultimately, the reduction in NEEC effectiveness can be understood, in part, as a byproduct of the study area not continuously accumulating biomass and instead seeing a steady reduction in biomass across every ecoregion over the course of the simulation.

Two ecoregions (Fig. 34) comprise most of the biomass across simulation ecoregion 10 and 5. These two ecoregions are more forested than the others, almost entirely within Los Padres National Forest, Los Angeles National Forest, and San Bernardino National Forest. These two regions tend to be within the highest elevation zones across the study area and are situated amongst most of the mixed conifer forests that are within the area of interest. These two regions also experienced the highest SOMC gain over simulation periods, and soil mineral nitrogen held within a range that the increasing carbon storage without increasing nitrogen storage reduced species

productivity (Cotrufo et al. 2019), possibly reducing biomass growth. In other ecoregions with less NEEC productivity and AGNPP, we see less SOMC gain and higher mineral nitrogen soil deposition throughout. Compared to ecoregions 5 and 10, I believe these nitrogen levels have limited species' productivity ability. This rapid growth of nitrogen in the soil starting from the beginning of the simulation period has caused species to grow excessively and not establish root systems, reducing the ability to store nutrients. While a relationship between too fast increasing mineral nitrogen and compared to soil carbon would reduce soil carbon (Mason-Jones, Schmücker, and Kuzyakov 2018).

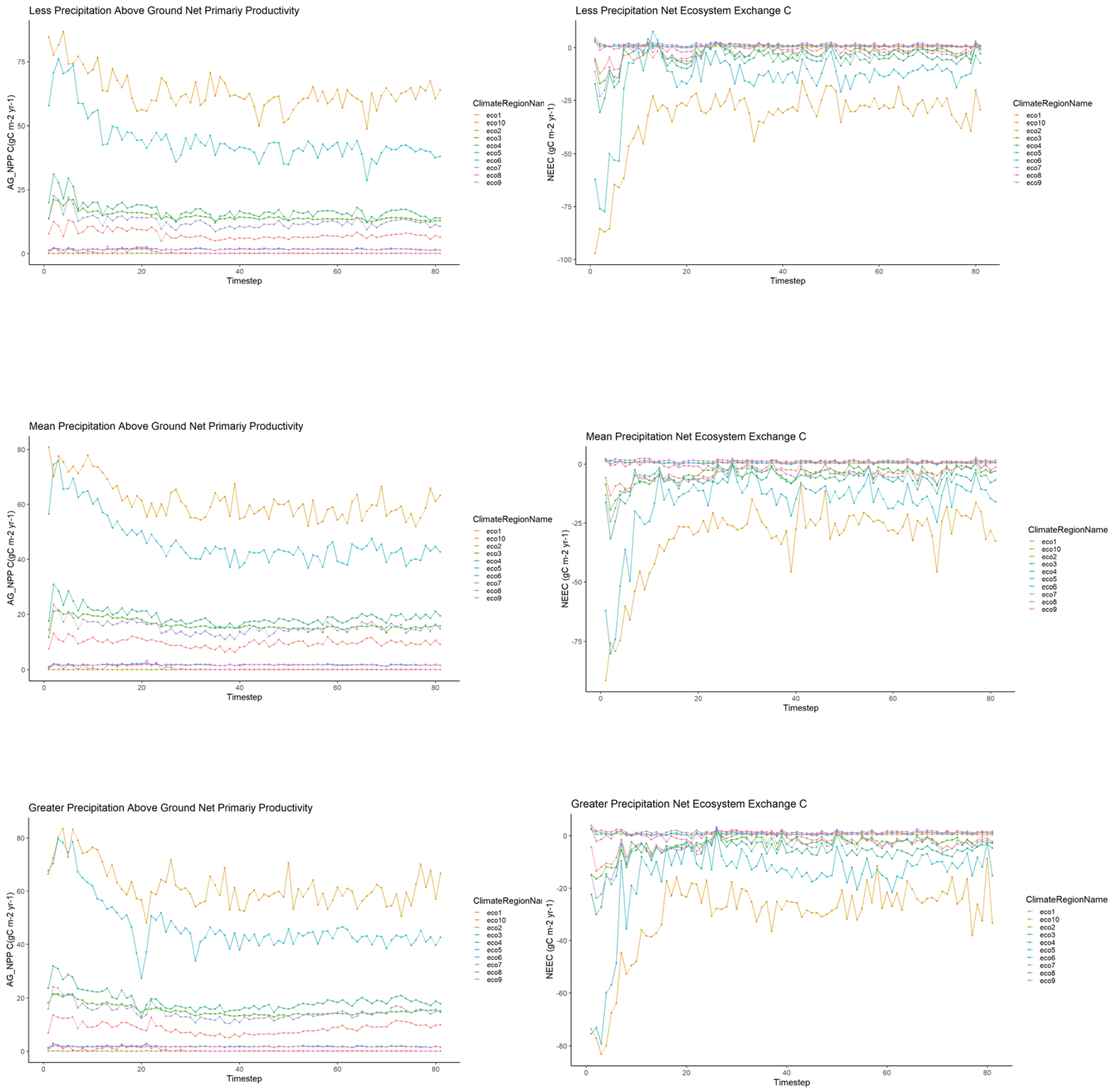


Fig. 28 – Graphs showing AGNPP and NEEC of all three climate scenarios.

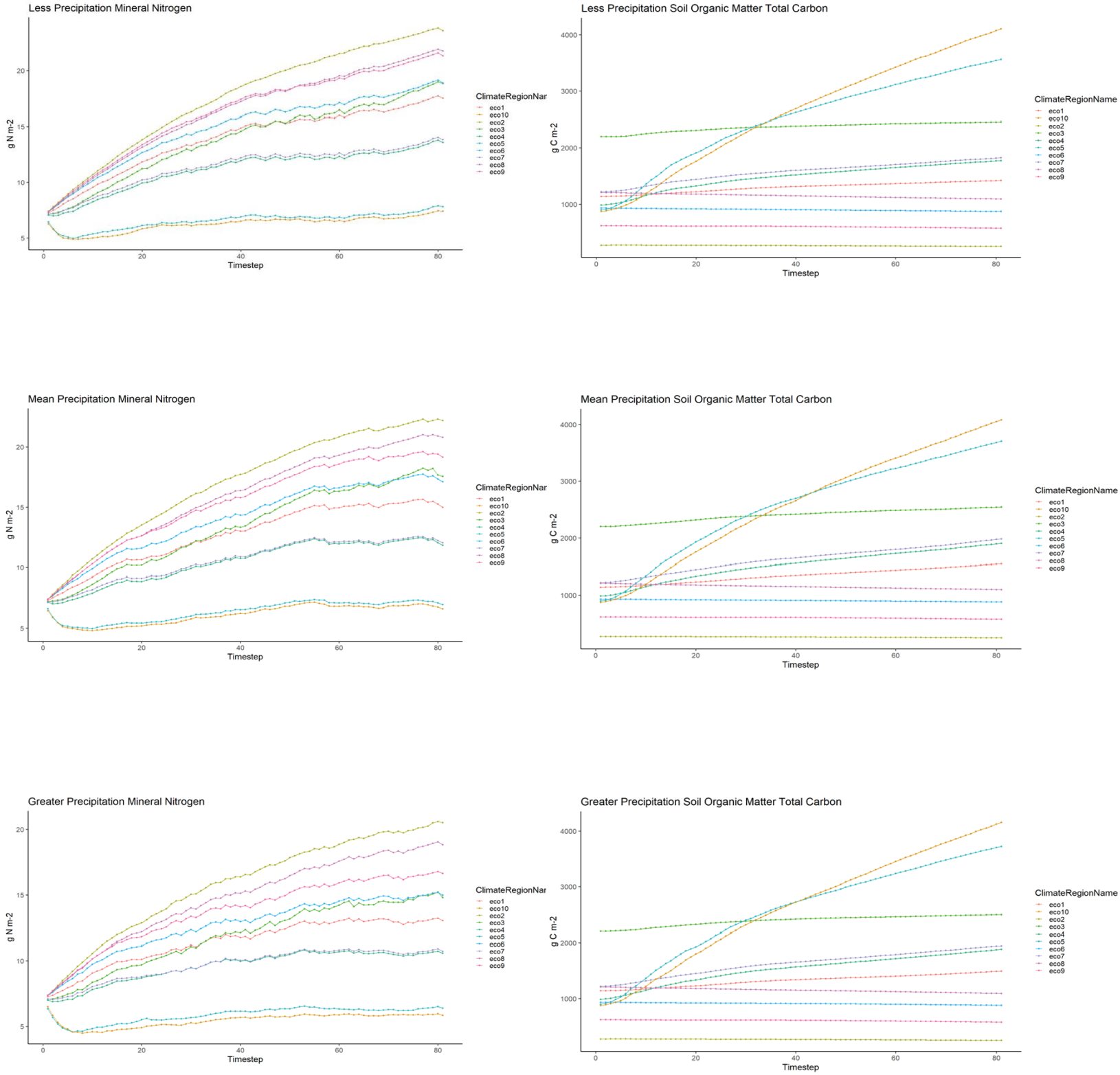


Fig. 29 – Graphs showing AGNPP and NEEC of all three climate scenarios.

Figure 28 shows ecosystem processes over the study through each climate scenario. *Greater* Precipitation starts with the highest NEEC, but landscape events eventually lead to a less productive study area. NEEC and AGNPP are very similar across each climate scenario, with some small differences across landscape runs. Figure 29 shows landscape soil organic matter total carbon and mineral nitrogen across each ecoregion. This figure shows an increasing mineral nitrogen deposition into landscape soils outside of ecoregion 5 and 10 which are also the most productive in terms of NEEC and AGNPP. SOMTC figures show a steady incline for ecoregion 5 and 10 while other regions decline or experience a slow increase over the simulation period.

Table 15 – mean aboveground net primary production and net ecosystem exchange of carbon.

| Climate Scenario | Mean AGNPP (g c m/2 - 1) | Mean NEEC (g c m/2 - 1) |
|---|---|---|
| *Greater Precipitation* | 17.04679 | -5.913457 |
| *Mean Precipitation* | 17.2087 | -6.331975 |
| *Less Precipitation* | 16.2953 | -5.764938 |

The results of forest succession across the landscape through each scenario suggest that part of the landscape may not be accurately parameterized, which can heavily impact the effects of fire interactions around the WUI and ultimately impact the results of my research question of how climate scenarios affect WUI burned area and frequency. Through the simulation and each climate scenario, the WUI experienced a similar or identical amount of fire, with less than 7% of the WUI not being impacted by fire in both 2050 and 2100. McKenzie & Littell 2016 and Liu & Wimberly 2016 both suggest that wildfire in the West is predicted to increase with global warming, which would explain the WUI burned area results. Keeley & Syphard 2016 indicate that in the short-term, increases in fire activity will drive decreases in fire due to fuel limitations

where this work saw the opposite. This work saw that 2100 WUI experienced more ignitions under the *Mean* and *Less Precipitation* scenarios with *Greater Precipitation* experiencing nearly the same amount of ignition as 2050 WUI. The greater ignitions in 2100 WUI all happened under a landscape with less biomass overall than starting conditions and a similar total burned area to 2050 WUI.

Throughout 2050, over the three scenarios, the WUI only saw fire low fire intensity where flame lengths would be < 4 feet and moderate fire intensity of 4- 8 feet flame lengths while high severity fires of > 8-foot flame lengths were not present in any simulation. A possibility of the WUI only experiencing low to moderate fire intensity could be from the lack of biomass or fuels across the landscape, which aligns with the suggestions of Keeley & Syphard 2016. One work found that fuels across the landscape and VPD were the most significant contributors to high-severity fires in California (Safford et al. 2022). The lack of early high severity fires could have resulted from an inaccurate, low, starting biomass (Zhao, Guo, and Kelly 2012) while reduction in biomass as the scenarios ran could have resulted in less severe wildfires being in line with predictions from Keeley & Syphard 2016.

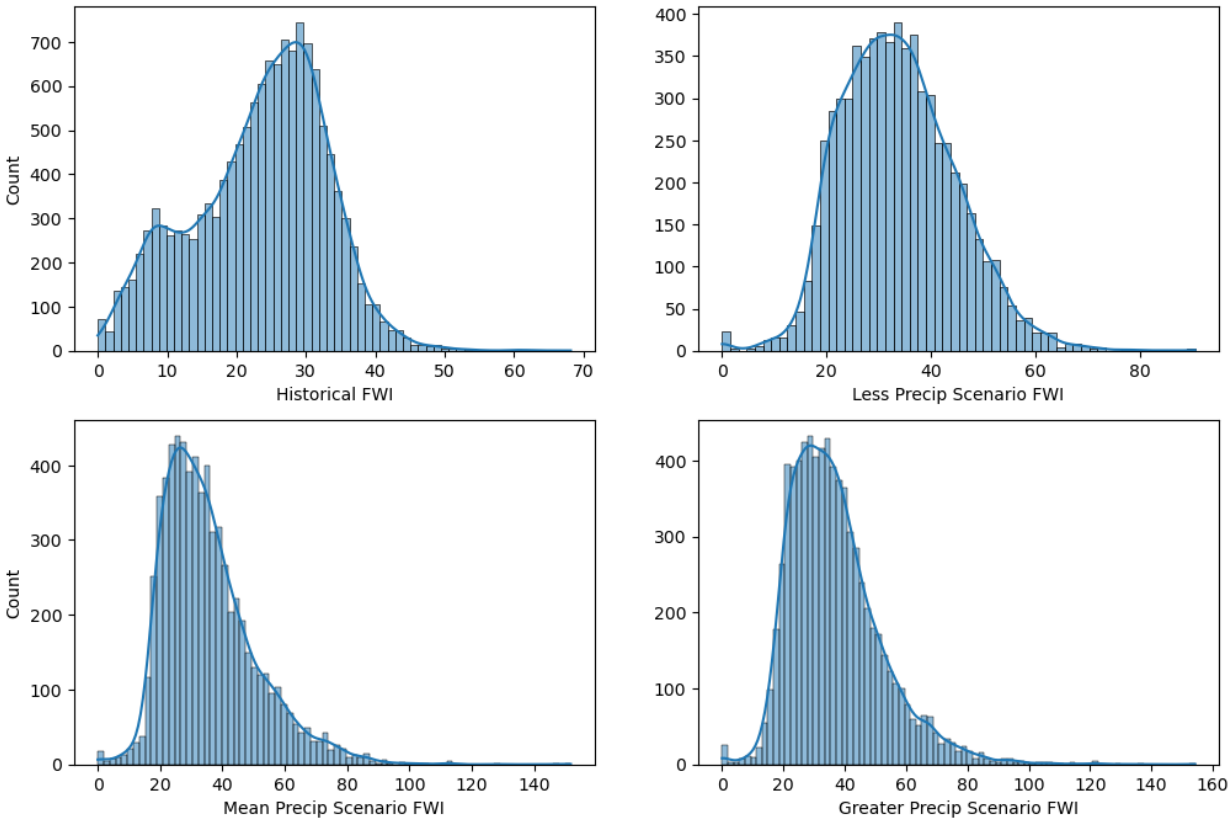


Fig. 30 – Graphs showing historical and future scenarios runs FWI.

Figure 30 shows one aspect of the historical climate data that was used to parameterize ignitions provided by Robbins (Personal Communications, 2022). Historical data of FWI was over 38 years (1979 - 2016) per each ecoregion, while the future scenarios FWI was calculated within SCRRPLE over the simulation. This figure shows the historical FWI and the FWI of the three climate scenarios used within the model. When future climate FWI was compared to historical FWI, we see a bimodal distribution of FWI, while future scenarios describe a unimodal distribution of FWI. The steeper initial incline of future climate scenarios' FWI could indicate that the suppression csv should be revisited to ensure correct parameterization to fit these curves. Looking further into climate with the scenario *Less Precipitation* saw the least number of ignitions within the WUI this might be explained as in southern California ignitions were

more frequent in areas with warmer temperatures and higher precipitation (Faivre et al. 2014).

There were limitations in this work. Throughout this simulation, it was impossible to simulate the feedback between projections of urban growth/wildland-urban interface areas and forest succession. Feedback between forest succession and urban growth will be an essential aspect to capture in future work as land use change is one of the most critical anthropogenic factors impacting ecosystems, with habitation loss, species changes, and altered fire regimes (Syphard, Clarke, and Franklin 2005) which is vital to note when understanding how WUI fires may impact future urban growth and forest succession. Another area for improvement in this work could be a misinterpretation of biomass across the landscape where starting biomass does not match biomass conditions experienced in other works. Spending more time adjusting species biomass will be essential to ensure I properly account for carbon across the landscape. One study suggests that within 36.1 km2, biomass ranged from 38.6 – 1132.9 mg/ha (Zhao, Guo, and Kelly 2012), while my ecoregions ranged at LANDIS-II time 0 .13 mg/ha to 51.12 mg/ha suggesting that there is still work to do.

In the future, I would like to adjust biomass to be more accurate to real-world scenarios to properly project forest succession and adjust mineral n throughout my ecoregions to encourage growth. I will achieve this by going through my source code and looking for possible errors while testing different biomass calculations. Mineral n can be easily adjusted through the NECN-succession text file, and it would be prudent to re-evaluate my mineral nitrogen soil pools. I would also like to see WUI growth under a different population growth model, which would be more in line with RCP 4.5, to

understand if that would change WUI fire dynamics when compared to the RCP 8.5 scenarios I ran the model on. This work did not capture the full stochastic nature of LANDIS through the power of replicate simulations. In the future I will run multiple runs with each scenario to create an average scenario to better understand the results of each model. I would like to add WUI interaction to the model as well, this may come in the form of where just climate changes, runs where the WUI changes, and runs where both changes, and finally where neither change. Then comparing the difference in each scenario to see if they are statistically different. I believe these changes would create a more holistic and accurate simulation of future fire in the southern Californian WUI.

## 6.2 Conclusion

This analysis answered my research question and suggested that fires will heavily impact the WUI across three different climate scenarios, with less than 7% of total WUI area remaining unscathed in both 2050 and 2100. Across all three climate scenarios the WUI only experienced low to moderate severity fire with all three experiencing nearly identical amounts of burned WUI area across low and moderate severity classes. The impact of fire is worryingly high for the region, which holds a large portion of California's economic function and population. As urban areas continue to expand, it will be increasingly important to assess housing growth in this region to limit exposure to WUI fire which has led to California experiencing its most extensive WUI fire-related structure loss in recent years (Syphard et al. 2019). It is increasingly important to consider how future population growth and land cover change may alter fire

regimes even further from the historical norm and what can be done to mitigate damage to life and property in this wildland-urban interface and intermix zones.

References

Abrahamson, Ilana, 2014. Fire Effects Information System (FEIS). Available online at https://www.feis-crs.org/feis/.

Abatzoglou, J. T. (2013), Development of gridded surface meteorological data for ecological applications and modelling. Int. J. Climatol., 33: 121–131.

Albrecht, R., S. Goodman, D. Buechler, R. Blakeslee, and H. Christian, 2016: Where Are the Lightning Hotspots on Earth?. Bull. Amer. Meteor. Soc., 97, 2051–2068, doi: 10.1175/BAMS-D-14-00193.1.

Ager, A. A., P. Palaiologou, C. R. Evers, M. A. Day, C. Ringo, and K. Short. 2019. Wildfire exposure to the wildland urban interface in the western US. *Applied Geography* 111:102059.

Airey Lauvaux, C., C. N. Skinner, and A. H. Taylor. 2016. High severity fire and mixed conifer forest-chaparral dynamics in the southern Cascade Range, USA. *Forest Ecology and Management* 363:74–85.

Balch, J. K., J. T. Abatzoglou, M. B. Joseph, M. J. Koontz, A. L. Mahood, J. McGlinchy, M. E. Cattau, and A. P. Williams. 2022. Warming weakens the night-time barrier to global fire. *Nature* 602 (7897):442–448.

Barry, D. 2014. Refining dendrochronology to evaluate the relationship between age and diameter for dominant riparian trees in the Redwood Creek watershed. :55.

Battles, J. J., T. Robards, A. Das, K. Waring, J. K. Gilless, G. Biging, and F. Schurr. 2008. Climate change impacts on forest growth and tree mortality: a data-driven modeling study in the mixed-conifer forest of the Sierra Nevada, California. *Climatic Change* 87 (S1):193–213.

Bisquay-Garcia, V. 2021. Forest management for climate adaptation: Effect of three management scenarios on the landscape disturbances and responses to climate change. *NC State University*.

Blodgett, David L., Nathaniel L. Booth, Thomas C. Kunicki, Jordan I. Walker, and Roland J. Viger. Description and testing of the Geo Data Portal: Data integration framework and Web processing services for environmental science collaboration. No. 2011-1157. US Geological Survey, 2011.

Brotherson, J. D., J. N. Davis, and L. Greenwood. 1980. Diameter-Age Relationships of Two Species of Mountain Mahogany. *Journal of Range Management* 33 (5):367–370.

Buechi, H., P. Weber, S. Heard, D. Cameron, A. J. Plantinga, H. Buechi, P. Weber, S. Heard, D. Cameron, and A. J. Plantinga. 2021. Long-term trends in wildfire damages in California. *International Journal of Wildland Fire* 30 (10):757–762.

Burge, D. O., J. H. Thorne, S. P. Harrison, B. C. O'Brien, J. P. Rebman, J. R. Shevock, E. R. Alverson, L. K. Hardison, J. D. RodrÍguez, S. A. Junak, T. A. Oberbauer, H. Riemann, S. E. Vanderplank, and T. Barry. 2016. Plant Diversity and Endemism in the California Floristic Province. *Madroño* 63 (2):3–206.

Ciceu, A., J. G. Duro, C. Aponte, I. S. Pascu, A. Claudiu-Dobre, V. Zamfira, Ş. Leca, D. Pitar, B. Apostol, E. N. Apostol, Ş. Chivulescu, and O. Badea. 2020. Landis-II simulation model integration in Romania's forest management. *Revista de Silvicultura si Cinegetica* 25 (46):47–55.

Cohen, J. 2008. The wildland-urban interface fire problem: A consequence of the fire exclusion paradigm. *Forest History Today. Fall: 20-26.* :20–26.

Comer, P., D. Faber-Langendoen, R. Evans, S. Gawler, C. Josse, G. Kittel, S. Menard, M. Pyne, M. Reid, K. Schulz, K. Snow, and J. Teague. 2003. Ecological Systems of the United States: A Working Classification of U.S. Terrestrial Systems. NatureServe, Arlington, Virginia.

Cotrufo, M. F., M. G. Ranalli, M. L. Haddix, J. Six, and E. Lugato. 2019. Soil carbon storage informed by particulate and mineral-associated organic matter. Nature Geoscience 12 (12):989–994.

Deak, A. 2022. SCRRPLE (fire). https://github.com/alideak/Project-Klamath-RxFire/tree/main/parameterization/SCRPPLE%20(fire)

De Jager, N. R., P. J. Drohan, B. M. Miranda, B. R. Sturtevant, S. L. Stout, A. A. Royo, E. J. Gustafson, and M. C. Romanski. 2017. Simulating ungulate herbivory across forest landscapes: A browsing extension for LANDIS-II. *Ecological Modelling* 350:11–29.

Erickson, A., and N. Strigul. 2019. A Forest Model Intercomparison Framework and Application at Two Temperate Forests Along the East Coast of the United States. *Forests* 10 (2):180.

Faivre, N., Y. Jin, M. L. Goulden, and J. T. Randerson. 2014. Controls on the spatial pattern of wildfire ignitions in Southern California. *International Journal of Wildland Fire* 23 (6):799.

Flannigan, M. D., B. M. Wotton, G. A. Marshall, W. J. de Groot, J. Johnston, N. Jurko, and A. S. Cantin. 2016. Fuel moisture sensitivity to temperature and precipitation: climate change implications. *Climatic Change* 134 (1):59–71.

Franklin, J. 2010. Vegetation dynamics and exotic plant invasion following high severity crown fire in a southern California conifer forest. *Plant Ecology* 207 (2):281–295.

Gascho Landis, A. M., and J. D. Bailey. 2006. Predicting Age of Pinyon and Juniper Using Allometric Relationships. *Western Journal of Applied Forestry* 21 (4):203–206.

Garrison, J. D., and T. E. Huxman. 2020. A tale of two suburbias: Turning up the heat in Southern California's flammable wildland-urban interface. *Cities* 104:102725.

Glickman, D. & Babbitt, B. Urban wildland interface communities within the vicinity of federal lands that are at high risk from wildfire. *Fed. Reg.* **66**, 751–777 (2001).

Gray, A. N., T. J. Brandeis, J. D. Shaw, W. H. McWilliams, and P. Miles. 2012. Forest Inventory and Analysis Database of the United States of America (FIA). *In: Dengler, J.;*

*Oldeland, J.; Jansen, F.; Chytry, M.; Ewald, J., Finckh, M.; Glockler, F.; Lopez-Gonzalez, G.; Peet, R. K.; Schaminee, J .H. J., eds. Vegetation databases for the 21st century. Biodiversity and Ecology. 4: 225-231.* :225–231.

Gray, A. N., H. S. J. Zald, R. A. Kern, and M. North. Stand Conditions Associated with Tree Regeneration in Sierran Mixed-Conifer Forests. :13.

Griffith, G.E., Omernik, J.M., Smith, D.W., Cook, T.D., Tallyn, E., Moseley, K., and Johnson, C.B., 2016, Ecoregions of California (poster): U.S. Geological Survey Open-File Report 2016–1021, with map, scale 1:1,100,000, http://dx.doi.org/10.3133/ofr20161021

Goss, M., D. L. Swain, J. T. Abatzoglou, A. Sarhadi, C. A. Kolden, A. P. Williams, and N. S. Diffenbaugh. 2020. Climate change is increasing the likelihood of extreme autumn wildfire conditions across California. *Environmental Research Letters* 15 (9):094016.

Guzman-Morales, J., and A. Gershunov. 2019. Climate Change Suppresses Santa Ana Winds of Southern California and Sharpens Their Seasonality. *Geophysical Research Letters* 46 (5):2772–2780.

Halsey, R. W., and J. E. Keeley. 2016. Conservation Issues: California Chaparral. In *Reference Module in Earth Systems and Environmental Sciences*, B9780124095489096000. Elsevier

https://linkinghub.elsevier.com/retrieve/pii/B9780124095489095841 (last accessed 2 August 2021).

Huang, J., M. S. Lucash, R. M. Scheller, and A. Klippel. 2021. Walking through the forests of the future: using data-driven virtual reality to visualize forests under climate change. *International Journal of Geographical Information Science* 35 (6):1155–1178.

Husari, S., H. T. Nichols, N. G. Sugihara, and S. L. Stephens. 2006. Fire and Fuel Management. In *Fire in California's Ecosystems*, ed. N. Sugihara, 444–465. University of California Press http://california.universitypressscholarship.com/view/10.1525/california/9780520246058.001.0001/upso-9780520246058-chapter-19 (last accessed 2 August 2021).

Jacobsen, A. L., S. D. Davis, and S. L. Fabritius. 2004. Fire frequency impacts non-sprouting chaparral shrubs in the Santa Monica Mountains of southern California. No pagination in
Ecology, conservation and management of Mediterranean climate ecosystems, Arianoutsou, M., and V. P. Panastasis (eds.). Millpress, Rotterdam, The Netherlands

Kanungo, T., D. M. Mount, N. S. Netanyahu, C. D. Piatko, R. Silverman, and A. Y. Wu. 2002. An efficient k-means clustering algorithm: analysis and implementation. *IEEE Transactions on Pattern Analysis and Machine Intelligence* 24 (7):881–892.

Keane, R. E., L. M. Holsinger, and S. D. Pratt. 2006. *Simulating historical landscape dynamics using the landscape fire succession model LANDSUM version 4.0*. Ft. Collins,

CO: U.S. Department of Agriculture, Forest Service, Rocky Mountain Research Station. https://www.fs.usda.gov/treesearch/pubs/22355 (last accessed 12 November 2021).

Keeley, J. E. 2002. Fire Management of California Shrubland Landscapes. *Environmental Management* 29 (3):395–408.

Keeley, J. E., C. J. Fotheringham, and M. Morais. 1999. Reexamining Fire Suppression Impacts on Brushland Fire Regimes. *Science* 284 (5421):1829–1832.

Keeley, J. E., J. Guzman-Morales, A. Gershunov, A. D. Syphard, D. Cayan, D. W. Pierce, M. Flannigan, and T. J. Brown. Ignitions explain more than temperature or precipitation in driving Santa Ana wind fires. *Science Advances* 7 (30):eabh2262.

Keeley, J. E., and J. G. Pausas. 2018. Evolution of 'smoke' induced seed germination in pyroendemic plants. *South African Journal of Botany* 115:251–255.

Keeley, J. E., and A. D. Syphard. 2016. Climate Change and Future Fire Regimes: Examples from California. *Geosciences* 6 (3):37.

Keeley, J. E., and P. H. Zedler. 2009. Large, high-intensity fire events in southern California shrublands: debunking the fine-grain age patch model. *Ecological Applications* 19 (1):69–94.

Kelly, A. E., and M. L. Goulden. 2008. Rapid shifts in plant distribution with recent climate change. *Proceedings of the National Academy of Sciences* 105 (33):11823–11826.

Krofcheck, D. J., M. D. Hurteau, R. M. Scheller, and E. L. Loudermilk. 2017. Restoring surface fire stabilizes forest carbon under extreme fire weather in the Sierra Nevada. *Ecosphere* 8 (1):e01663.

Konings, A. G., A. P. Williams, and P. Gentine. 2017. Sensitivity of grassland productivity to aridity controlled by stomatal and xylem regulation. *Nature Geoscience* 10 (4):284–288.

Kozak, A., and R. C. Yang. 1981. Equations for Estimating Bark Volume and Thickness of Commercial Trees in British Columbia. *The Forestry Chronicle* 57 (3):112–115.

LANDFIRE, Earth Resources Observation and Science Center (EROS), U.S. Geological Survey. 2022. LANDFIRE 2020 Existing Vegetation Cover (EVC) CONUS 2022 Capable

Li, H., M. Kanamitsu, S.-Y. Hong, K. Yoshimura, D. R. Cayan, V. Misra, and L. Sun. 2014. Projected climate change scenario over California by a regional ocean–atmosphere coupled model system. *Climatic Change* 122 (4):609–619.

Liang, S., M. D. Hurteau, and A. L. Westerling. 2017. Response of Sierra Nevada forests to projected climate–wildfire interactions. *Global Change Biology* 23 (5):2016–2030.

Lindroth, A., L. Klemedtsson, A. Grelle, P. Weslien, and O. Langvall. 2008. Measurement of net ecosystem exchange, productivity and respiration in three spruce

forests in Sweden shows unexpectedly large soil carbon losses. *Biogeochemistry* 89 (1):43–60.

Liu, Z., and M. C. Wimberly. 2016. Direct and indirect effects of climate change on projected future fire regimes in the western United States. *Science of The Total Environment* 542:65–75.

Lippitt, C. L., D. A. Stow, J. F. O'Leary, J. Franklin, C. L. Lippitt, D. A. Stow, J. F. O'Leary, and J. Franklin. 2012. Influence of short-interval fire occurrence on post-fire recovery of fire-prone shrublands in California, USA. *International Journal of Wildland Fire* 22 (2):184–193.

Lucash, M. S., R. M. Scheller, E. J. Gustafson, and B. R. Sturtevant. 2017. Spatial resilience of forested landscapes under climate change and management. *Landscape Ecology* 32 (5):953–969.

Lorek, H., and M. Sonnenschein. 1998. Object-oriented support for modelling and simulation of individual-oriented ecological models. *Ecological Modelling* 108 (1):77–96.

Ma, Q., Y. Su, S. Tao, and Q. Guo. 2018. Quantifying individual tree growth and tree competition using bi-temporal airborne laser scanning data: a case study in the Sierra Nevada Mountains, California. *International Journal of Digital Earth* 11 (5):485–503.

McDonald, P. M. 1983. *Local Volume Tables for Pacific Madrone, Tanoak, and California Black Oak in North-central California*. U.S. Department of Agriculture, Forest Service, Pacific Southwest Forest and Range Experiment Station.

Mairota, P., V. Leronni, W. Xi, D. Mladenoff, and H. Nagendra. 2013. Using spatial simulations of habitat modification for adaptive management of protected areas: Mediterranean grassland modification by woody plant encroachment. *Environmental Conservation* 41.

Mason-Jones, K., N. Schmücker, and Y. Kuzyakov. 2018. Contrasting effects of organic and mineral nitrogen challenge the N-Mining Hypothesis for soil organic matter priming. Soil Biology and Biochemistry 124:38–46.

Martinuzzi, S., S. I. Stewart, D. P. Helmers, M. H. Mockrin, R. B. Hammer, and V. C. Radeloff. 2015. *The 2010 wildland-urban interface of the conterminous United States*. Newtown Square, PA: U.S. Department of Agriculture, Forest Service, Northern Research Station. https://www.fs.usda.gov/treesearch/pubs/48642 (last accessed 14 September 2022).

Maxwell, C., R. Scheller, J. Long, and P. Manley. 2022. Forest management under uncertainty: the influence of management versus climate change and wildfire in the Lake Tahoe Basin, USA. *Ecology and Society* 27 (2). https://ecologyandsociety.org/vol27/iss2/art15 (last accessed 14 July 2022).

McKenzie, D., and J. S. Littell. 2017. Climate change and the eco-hydrology of fire: Will area burned increase in a warming western USA? *Ecological Applications* 27 (1):26–36.

Miller, J. D., H. D. Safford, M. Crimmins, and A. E. Thode. 2009. Quantitative Evidence for Increasing Forest Fire Severity in the Sierra Nevada and Southern Cascade Mountains, California and Nevada, USA. *Ecosystems* 12 (1):16–32.

Miller, J. D., C. N. Skinner, H. D. Safford, E. E. Knapp, and C. M. Ramirez. 2012. Trends and causes of severity, size, and number of fires in northwestern California, USA. *Ecological Applications* 22 (1):184–203.

Minnich, R. A. 1983. Fire Mosaics in Southern California and Northern Baja California. *Science* 219 (4590):1287–1294.

Minnich, R. A., M. G. Barbour, J. H. Burk, and R. F. Fernau. 1995. Sixty Years of Change in Californian Conifer Forests of the San Bernardino Mountains. *Conservation Biology* 9 (4):902–914.

Mladenoff, D. J. 2004. LANDIS and forest landscape models. *Ecological Modelling* 180 (1):7–19.

Marutho, D., S. Hendra Handaka, E. Wijaya, and Muljono. 2018. The Determination of Cluster Number at k-Mean Using Elbow Method and Purity Evaluation on Headline News. In *2018 International Seminar on Application for Technology of Information and Communication*, 533–538.

Nigro, K., and N. Molinari. 2019. Status and trends of fire activity in southern California yellow pine and mixed conifer forests. *Forest Ecology and Management* 441:20–31.

Omernik, J.M. 1987. Ecoregions of the conterminous United States. Map (scale 1:7,500,000). Annals of the Association of American Geographers 77(1):118-125.

Parks, S. A., C. Miller, J. T. Abatzoglou, L. M. Holsinger, M.-A. Parisien, and S. Z. Dobrowski. 2016. How will climate change affect wildland fire severity in the western US? *Environmental Research Letters* 11 (3):035002.

Parton, W. J. 1996. The CENTURY model. In *Evaluation of Soil Organic Matter Models*, NATO ASI Series., eds. D. S. Powlson, P. Smith, and J. U. Smith, 283–291. Berlin, Heidelberg: Springer.

Paudel, A., M. Coppoletta, K. Merriam, and S. H. Markwith. 2022. Persistent composition legacy and rapid structural change following successive fires in Sierra Nevada mixed conifer forests. *Forest Ecology and Management* 509:120079.

Pierce, D. W., D. R. Cayan, T. Das, E. P. Maurer, N. L. Miller, Y. Bao, M. Kanamitsu, K. Yoshimura, M. A. Snyder, L. C. Sloan, G. Franco, and M. Tyree. 2013. The Key Role of Heavy Precipitation Events in Climate Model Disagreements of Future Annual Precipitation Changes in California. *Journal of Climate* 26 (16):5879–5896.

Polade, S. D., D. W. Pierce, D. R. Cayan, A. Gershunov, and M. D. Dettinger. 2014. The key role of dry days in changing regional climate and precipitation regimes. *Scientific Reports* 4 (1):4364.

Price, O., and R. Bradstock. 2014. Countervailing effects of urbanization and vegetation extent on fire frequency on the Wildland Urban Interface: Disentangling fuel and ignition effects. *Landscape and Urban Planning* 130:81–88.

PRISM Climate Group, Oregon State University, https://prism.oregonstate.edu.

QGIS.org. 2022. QGIS Geographic Information System. QGIS Association. http://www.qgis.org

Radeloff, V. C., R. B. Hammer, S. I. Stewart, J. S. Fried, S. S. Holcomb, and J. F. McKeefry. 2005. THE WILDLAND–URBAN INTERFACE IN THE UNITED STATES. *Ecological Applications* 15 (3):799–805.

Radeloff, V. C., D. P. Helmers, H. A. Kramer, M. H. Mockrin, P. M. Alexandre, A. Bar-Massada, V. Butsic, T. J. Hawbaker, S. Martinuzzi, A. D. Syphard, and S. I. Stewart. 2018. Rapid growth of the US wildland-urban interface raises wildfire risk. *Proceedings of the National Academy of Sciences of the United States of America* 115 (13):3314–3319.

R Core Team. 2022. R: A language and environment for statistical computing. R Foundation for Statistical Computing, Vienna, Austria. URL https://www.R-project.org/.

Rebain, Stephanie A. comp. 2010 (revised February 1, 2022). The Fire and Fuels Extension to the Forest Vegetation Simulator: Updated Model Documentation. Internal Rep. Fort Collins, CO: U. S. Department of Agriculture, Forest Service, Forest Management Service Center. 409p.

Riley, Karin L.; Grenfell, Isaac C.; Finney, Mark A.; Wiener, Jason M.; Houtman, Rachel M. 2019. Fire Lab tree list: A tree-level model of the conterminous United States landscape circa 2014. Fort Collins, CO: Forest Service Research Data Archive. https://doi.org/10.2737/RDS-2019-0026.

Rupp, T. S., A. M. Starfield, and F. S. Chapin. A frame-based spatially explicit model of subarctic vegetation response to climatic change: comparison with a point model. :18.

Robbins, Z. J. 2022. Interactions among Climate, Disturbance, and Forests Will Shape Future Landscapes.

Robbins, Z. J., Loudermilk, E. L., Reilly, M. J., O'Brien, J. J., Jones, K., Gerstle, C. T., & Scheller, R. M. (2022). Delayed fire mortality has long-term ecological effects across the Southern Appalachian landscape. *Ecosphere, 13(6), e4153.*

Safford, H. D., D. A. Schmidt, and C. H. Carlson. 2009. Effects of fuel treatments on fire severity in an area of wildland–urban interface, Angora Fire, Lake Tahoe Basin, California. *Forest Ecology and Management* 258 (5):773–787.

Safford, H. D., A. K. Paulson, Z. L. Steel, D. J. N. Young, and R. B. Wayman. 2022. The 2020 California fire season: A year like no other, a return to the past or a harbinger of the future? *Global Ecology and Biogeography* 31 (10):2005–2025.

Safford, H. D., and J. T. Stevens. 2017. *Natural range of variation for yellow pine and mixed-conifer forests in the Sierra Nevada, southern Cascades, and Modoc and Inyo National Forests, California, USA*. Albany, CA: U.S. Department of Agriculture, Forest

Service, Pacific Southwest Research Station. https://www.fs.usda.gov/treesearch/pubs/55393 (last accessed 10 August 2021).

Sandel, B., and E. M. Dangremond. 2012. Climate change and the invasion of California by grasses. *Global Change Biology* 18 (1):277–289.

Schafer, J. L., B. P. Breslow, M. G. Hohmann, and W. A. Hoffmann. 2015. Relative Bark Thickness is Correlated with Tree Species Distributions along a Fire Frequency Gradient. *Fire Ecology* 11 (1):74–87.

Schrader-Patton, C. C., and E. C. Underwood. 2021. New Biomass Estimates for Chaparral-Dominated Southern California Landscapes. *Remote Sensing* 13 (8):1581.

Scheller, R., A. Kretchun, T. J. Hawbaker, and P. D. Henne. 2019. A landscape model of variable social-ecological fire regimes. *Ecological Modelling* 401:85–93.

Scheller, R., M. S. Lucash, A. Kretchun, P. Henne, C. Haga, W. Hotta. 2022. LANDIS-II SCRAPPLE Extension v2.3.

Scheller, R. M., J. B. Domingo, B. R. Sturtevant, J. S. Williams, A. Rudy, E. J. Gustafson, and D. J. Mladenoff. 2007. Design, development, and application of LANDIS-II, a spatial landscape simulation model with flexible temporal and spatial resolution. *Ecological Modelling* 201 (3):409–419.

Scheller, R.M., D. Hua, P.V. Bolstad, R. Birdsey, D.J. Mladenoff. 2011. The effects of forest harvest intensity in combination with wind disturbance on carbon dynamics in a Lake States mesic landscape. Ecological Modelling 222: 144-153.

Scheller, R. M., M. S. Lucash, A. Kretchun, P. Henne, C. Haga, and W. Hotta. 2022. LANDIS-II Net Ecosystem Carbon and Nitrogen (NECN) Succession v6.8 Extension User Guide. :33.

Scheller, R.M., W.D. Spencer, H. Rustigian-Romsos, A.D.Syphard, B.C. Ward, J.R. Strittholt. 2011. Using stochastic simulation to evaluate competing risks of wildfires and fuels management on an isolated forest carnivore. Landscape Ecology 26: 1491-1504.

Schoennagel, T., J. K. Balch, H. Brenkert-Smith, P. E. Dennison, B. J. Harvey, M. A. Krawchuk, N. Mietkiewicz, P. Morgan, M. A. Moritz, R. Rasker, M. G. Turner, and C. Whitlock. 2017. Adapt to more wildfire in western North American forests as climate changes. *Proceedings of the National Academy of Sciences* 114 (18):4582–4590.

Short, Karen C. 2021. Spatial wildfire occurrence data for the United States, 1992-2018 [FPA_FOD_20210617]. 5th Edition. Fort Collins, CO: Forest Service Research Data Archive. https://doi.org/10.2737/RDS-2013-0009.5

Singh, D., and B. Singh. 2020. Investigating the impact of data normalization on classification performance. *Applied Soft Computing* 97:105524.

Sleeter, B. M., and T. T. Wilson. 2017. Land-use and Land-cover Projections for California's 4th Climate Assessment. https://www.sciencebase.gov/catalog/item/587fb408e4b085de6c11f389 (last accessed 21 September 2022).

Spencer, W.D., H. Rustigan, R.M. Scheller, J.R. Strittholt,W.J. Zielinski, and R. Truex. 2011. Using occupancy and population models to assess habitat conservation opportunities for an isolated carnivore population.Biological Conservation 144: 788-803.

Stavros, E. N., J. T. Abatzoglou, D. McKenzie, and N. K. Larkin. 2014. Regional projections of the likelihood of very large wildland fires under a changing climate in the contiguous Western United States. *Climatic Change* 126 (3):455–468.

Steel, Z. L., M. J. Koontz, and H. D. Safford. 2018. The changing landscape of wildfire: burn pattern trends and implications for California's yellow pine and mixed conifer forests. *Landscape Ecology* 33 (7):1159–1176.

Steel, Z. L., H. D. Safford, and J. H. Viers. 2015. The fire frequency-severity relationship and the legacy of fire suppression in California forests. *Ecosphere* 6 (1):art8.

Steele, J. H. 1989. The ocean 'landscape.' Landscape Ecology 3 (3):185–192.

Stephens, S. L., B. M. Collins, C. J. Fettig, M. A. Finney, C. M. Hoffman, E. E. Knapp, M. P. North, H. Safford, and R. B. Wayman. 2018. Drought, Tree Mortality, and Wildfire in Forests Adapted to Frequent Fire. *BioScience* 68 (2):77–88.

Sohl, T. L., K. L. Sayler, M. A. Bouchard, R. R. Reker, A. M. Friesz, S. L. Bennett, B. M. Sleeter, R. R. Sleeter, T. Wilson, C. Soulard, M. Knuppe, and T. Van Hofwegen. 2014. Spatially explicit modeling of 1992–2100 land cover and forest stand age for the conterminous United States. *Ecological Applications* 24 (5):1015–1036.

Soil Survey Staff. Gridded Soil Survey Geographic (gSSURGO) Database for the Conterminous United States. United States Department of Agriculture, Natural Resources Conservation Service. Available online at https://gdg.sc.egov.usda.gov/. November 16, 2020 (202007 official release).

Swain, D. L., B. Langenbrunner, J. D. Neelin, and A. Hall. 2018. Increasing precipitation volatility in twenty-first-century California. *Nature Climate Change* 8 (5):427–433.

Syakur, M. A., B. K. Khotimah, E. M. S. Rochman, and B. D. Satoto. 2018. Integration K-Means Clustering Method and Elbow Method For Identification of The Best Customer Profile Cluster. *IOP Conference Series: Materials Science and Engineering* 336:012017.

Sykes, M. T. 2009. Climate Change Impacts: Vegetation. In *Encyclopedia of Life Sciences*. John Wiley & Sons, Ltd https://onlinelibrary.wiley.com/doi/abs/10.1002/9780470015902.a0021227.

Syphard, A. D., T. J. Brennan, and J. E. Keeley. 2018. Chaparral Landscape Conversion in Southern California. In *Valuing Chaparral: Ecological, Socio-Economic, and Management Perspectives*, Springer Series on Environmental Management., eds. E. C. Underwood, H. D. Safford, N. A. Molinari, and J. E. Keeley, 323–346. Cham:

Springer International Publishing https://doi.org/10.1007/978-3-319-68303-4_12 (last accessed 10 August 2021).

Syphard, A.D., T. J. Brennan, and J. E. Keeley. 2019. Extent and drivers of vegetation type conversion in Southern California chaparral. *Ecosphere* 10 (7):e02796.

Syphard, A. D., K. C. Clarke, and J. Franklin. 2007. Simulating fire frequency and urban growth in southern California coastal shrublands, USA. *Landscape Ecology* 22 (3):431–445.

Syphard, A. D., K. C. Clarke, and J. Franklin. 2005. Using a cellular automaton model to forecast the effects of urban growth on habitat pattern in southern California. *Ecological Complexity* 2 (2):185–203.

Syphard, A. D., J. Franklin, and J. E. Keeley. 2006. Simulating the Effects of Frequent Fire on Southern California Coastal Shrublands. *Ecological Applications* 16 (5):1744–1756.

Syphard, A. D., V. C. Radeloff, J. E. Keeley, T. J. Hawbaker, M. K. Clayton, S. I. Stewart, and R. B. Hammer. 2007. Human Influence on California Fire Regimes. *Ecological Applications* 17 (5):1388–1402.

Syphard, A. D., H. Rustigian-Romsos, M. Mann, E. Conlisk, M. A. Moritz, and D. Ackerly. 2019. The relative influence of climate and housing development on current and projected future fire patterns and structure loss across three California landscapes. *Global Environmental Change* 56:41–55.

Syphard, A. D., R. M. Scheller, B. C. Ward, W. D. Spencer, J. R. Strittholt, A. D. Syphard, R. M. Scheller, B. C. Ward, W. D. Spencer, and J. R. Strittholt. 2011. Simulating landscape-scale effects of fuels treatments in the Sierra Nevada, California, USA. *International Journal of Wildland Fire* 20 (3):364–383.

Syphard, A. D., T. J. Brennan, H. Rustigian-Romsos, and J. E. Keeley. Fire-driven vegetation type conversion in Southern California. *Ecological Applications* n/a (n/a):e2626.

Talluto, M. V., and K. N. Suding. 2008. Historical change in coastal sage scrub in southern California, USA in relation to fire frequency and air pollution. *Landscape Ecology* 23 (7):803–815.

2019 TIGER/Line Shapefiles (machine-readable data files) / prepared by the U.S. Census Bureau, 2019

U.S. Geological Survey, USDA Forest Service, Nelson, K., 2021, Monitoring Trends in Burn Severity (ver. 4.0, March 2023): U.S. Geological Survey data release, https://doi.org/10.5066/P9IED7RZ.

U.S. Geological Survey (USGS) Gap Analysis Project (GAP), 2016, GAP/LANDFIRE National Terrestrial Ecosystems 2011: U.S. Geological Survey data release, https://doi.org/10.5066/F7ZS2TM0

U.S. Geological Survey (USGS). 2020. 1 Arc-second Digital Elevation Models (DEMs) - USGS National Map 3DEP Downloadable Data Collection. https://data.usgs.gov/datacatalog/data/USGS:35f9c4d4-b113-4c8d-8691-47c428c29a5b

Van de Water, K. M., and H. D. Safford. 2011. A Summary of Fire Frequency Estimates for California Vegetation before Euro-American Settlement. *Fire Ecology* 7 (3):26–58.

Vankat, J. L., and J. Major. 1978. Vegetation Changes in Sequoia National Park, California. *Journal of Biogeography* 5 (4):377–402.

Wagner, C. E. V. STRUCTURE OF THE CANADIAN FOREST FIRE WEATHER INDEX. :49.

Walters, S. P., Schneider, N. J., & Guthrie, J. D. (2011). Geospatial Multi-Agency Coordination (GeoMAC) wildland fire perimeters, 2008. In Data Series (No. 612). U.S. Geological Survey. https://doi.org/10.3133/ds612

Weinstein, D. A., and P. B. Woodbury. Review of Methods for Developing Probabilistic Risk Assessments. Part 1: Modeling Fire. :18.

Westerling, A. L. 2016. Increasing western US forest wildfire activity: sensitivity to changes in the timing of spring. *Philosophical Transactions of the Royal Society B: Biological Sciences* 371 (1696):20150178.

Westerling, A. L., H. G. Hidalgo, D. R. Cayan, and T. W. Swetnam. 2006. Warming and Earlier Spring Increase Western U.S. Forest Wildfire Activity. *Science* 313 (5789):940–943.

West, T.O. 2014. Soil Carbon Estimates in 20-cm Layers to 1-meter Depth, Conterminous US, 1970-1993. ORNL DAAC, Oak Ridge, Tennessee, USA. https://doi.org/10.3334/ORNLDAAC/1238.

Wiens, J. A., and B. T. Milne. 1989. Scaling of 'landscapes' in landscape ecology, or, landscape ecology from a beetle's perspective. Landscape Ecology 3 (2):87–96.

Williams, A. P., C. D. Allen, A. K. Macalady, D. Griffin, C. A. Woodhouse, D. M. Meko, T. W. Swetnam, S. A. Rauscher, R. Seager, H. D. Grissino-Mayer, J. S. Dean, E. R. Cook, C. Gangodagamage, M. Cai, and N. G. McDowell. 2013. Temperature as a potent driver of regional forest drought stress and tree mortality. *Nature Climate Change* 3 (3):292–297.

Williams, A. P., C. D. Allen, C. I. Millar, T. W. Swetnam, J. Michaelsen, C. J. Still, and S. W. Leavitt. 2010. Forest responses to increasing aridity and warmth in the southwestern United States. *Proceedings of the National Academy of Sciences* 107 (50):21289–21294.

Williams, A. P., J. T. Abatzoglou, A. Gershunov, J. Guzman-Morales, D. A. Bishop, J. K. Balch, and D. P. Lettenmaier. 2019. Observed Impacts of Anthropogenic Climate Change on Wildfire in California. *Earth's Future* 7 (8):892–910.

Voldoire, A., E. Sanchez-Gomez, D. Salas y Mélia, B. Decharme, C. Cassou, S. Sénési, S. Valcke, I. Beau, A. Alias, M. Chevallier, M. Déqué, J. Deshayes, H. Douville, E. Fernandez, G. Madec, E. Maisonnave, M.-P. Moine, S. Planton, D. Saint-Martin, S.

Szopa, S. Tyteca, R. Alkama, S. Belamari, A. Braun, L. Coquart, and F. Chauvin. 2013. The CNRM-CM5.1 global climate model: description and basic evaluation. *Climate Dynamics* 40 (9):2091–2121.

Yeh, H.-Y., and L. C. Wensel. 2000. The relationship between tree diameter growth and climate for coniferous species in northern California. *Canadian Journal of Forest Research* 30 (9):1463–1471.

Yuan, W., Y. Zheng, S. Piao, P. Ciais, D. Lombardozzi, Y. Wang, Y. Ryu, G. Chen, W. Dong, Z. Hu, A. K. Jain, C. Jiang, E. Kato, S. Li, S. Lienert, S. Liu, J. E. M. S. Nabel, Z. Qin, T. Quine, S. Sitch, W. K. Smith, F. Wang, C. Wu, Z. Xiao, and S. Yang. 2019. Increased atmospheric vapor pressure deficit reduces global vegetation growth. *Science Advances* 5 (8):eaax1396.

Zeibig-Kichas, N. E., C. W. Ardis, J.-P. Berrill, and J. P. King. 2016. Bark Thickness Equations for Mixed-Conifer Forest Type in Klamath and Sierra Nevada Mountains of California. *International Journal of Forestry Research* 2016:e1864039.

Zhao, F., Q. Guo, and M. Kelly. 2012. Allometric equation choice impacts lidar-based forest biomass estimates: A case study from the Sierra National Forest, CA. *Agricultural and Forest Meteorology* 165:64–72.